COMPLEX HIGH-STRAIN DEFORMATION IN THE USAGARAN OROGEN, TANZANIA: STRUCTURAL SETTING OF PALAEOPROTEROZOIC ECLOGITES

S.M. Reddy[1], A.S. Collins[1] & A. Mruma[2]

(1) Tectonics Special Research Centre, Department of Applied Geology, Curtin University of Technology, PO Box U1987, Perth, WA 6845, Australia.

(2) Department of Geology, University of Dar es Salaam, PO Box 35052, Dar es Salaam, Tanzania.

Key Words: kinematic evolution, Usagaran orogen, transpression, shear zone, U-Pb SHRIMP geochronology, Palaeoproterozoic tectonics.

* Corresponding author. Tel.:+61-8-9266-4371; fax: +61-8-9266-3153

E-mail address: sreddy@lithos.curtin.edu.au (S. Reddy)

Abstract

The Palaeoproterozoic Usagaran orogenic belt of Tanzania contains the Earth's oldest reported examples of subduction-related eclogite facies rocks. Detailed field mapping of gneisses exposed in the high-grade, eclogite-bearing part of the orogen (the Isimani Suite) indicates a complex deformation and thermal history. Deformation in the Isimani Suite can be broadly subdivided into five events. The first of these (D_1), associated with formation of eclogite facies metamorphism, is strongly overprinted by a pervasive deformation (D_2) at amphibolite facies conditions, which resulted in the accumulation of high strains throughout all of the exposed Isimani rocks. The geometry of foliations and lineations developed during D_2 deformation are variable and have different shear directions that enable five D_2 domains to be identified. Analysis of these domains indicates a geometrical and kinematic pattern that is interpreted to have formed by strain and kinematic partitioning during sinistral transpression. U-Pb SHRIMP zircon ages from a post-D_2 granite and previously published geochronological data from the Usagaran eclogites indicate this deformation took place between 2001 - 1.870 Ma (at maximum error). Subsequent greenschist facies deformation, localised as shear zones on boundaries separating D_2 domains have both contractional and extensional geometries that indicate post 1877 Ma reactivation of the Isimani Suite. This reactivation may have taken place during Palaeoproterozoic exhumation of the Usagaran Orogen or may be the result of deformation associated with the Neoproterozoic East African Orogen.

U-Th-Pb SHRIMP zircon ages from an Isimani gneiss sample and xenocrysts in a "post-tectonic" granite yield ~2.7 Ga ages and are similar to published Nd model ages from both the Tanzanian craton and gneiss exposed east of the Usagaran belt in the East African Orogen. These age data indicate that the Isimani Suite of the Usagaran Orogen reflects reworking of Archaean continental crust. The extensive distribution of ~2.7 Ga crust in both the footwall and hangingwall of the Usagaran Orogen can only be explained by the collision of two continents if the continents fortuitously had the same protolith ages. We propose that a more likely scenario is that the protoliths of the mafic eclogites were erupted in a marginal basin setting as either oceanic crust, or as limited extrusions along the rifted margin of the Tanzanian Craton. The Usagaran Orogen may therefore reflect the mid-Palaeoproterozoic reassembly of a continental ribbon partially or completely rifted off the craton and separated from it by a marginal basin.

Introduction

Eclogite facies rocks formed at low to medium temperatures (<900°C) and high pressures (>12 kbar) are characteristic of metamorphism within the down-going plate of subduction complexes (Ernst, 1971). They require low geothermal gradients to form and require sufficiently rapid exhumation rates that preclude retrograde metamorphic overprinting. Eclogite-facies rocks are relatively common in Phanerozoic orogens and their study has lead to significant advances in the understanding of the thermal-tectonic evolution of subduction systems (Ernst, 1971; Barnicoat and Fry, 1986; Peacock, 1993) and the processes and rates by which metamorphic rocks are exhumed in general (Platt, 1993a; Reddy et al., 1999; Ring et al., 1999). The fact that no low/medium temperature eclogites older than 2.0 Ga have been found, despite there being large regions of Archaean orogenesis with little or no subsequent reworking (c.f. De Roever, 1956), suggests that geological processes before this time, either those involved in plate subduction and collision, or the style and rate of exhumation, differed significantly from those that have operated since the Palaeoproterozoic.

The Palaeoproterozoic Usagaran Orogen of Tanzania (Fig. 1) contains eclogite-facies rocks that were metamorphosed to pressures of ~18 kbar and temperatures of ~750°C at 2000±1 Ma (Möller et al., 1995). This makes them the oldest known low-medium temperature eclogites, ~100 Ma older than the oldest examples in the Lapland Granulite Belt (Tuisku and Huhma, 1998). Their mid-ocean ridge basalt (MORB) like immobile element composition led Möller et al. (1995) to suggest that they represented slices of oceanic crust metamorphosed in a subduction system. Thermobarometric, geochemical and geochronological data from these eclogites have already been published (Möller et al., 1995). However, there is little structural data published from the Usagaran Orogen, and what data there are do not constrain the kinematic evolution of the Usagaran rocks. In this study, we consider the structural evolution of ancient eclogite-bearing rocks from the Usagaran orogen. We present a detailed structural analysis of the Isimani Suite where it is very well exposed in the Great Ruaha River section directly east of the Tanzanian Craton in central Tanzania (Fig. 1). This suite of rocks lies ~15 km along strike from the Yalumba Hill eclogites (Fig. 2) and contains retrogressed equivalents of high pressure rocks. We also integrate spatial and kinematic structural data with new zircon U-Pb SHRIMP analyses to place temporal constraints on the structural

evolution of the orogen. A detailed geochronological study involving U-Pb SHRIMP and $^{40}Ar/^{39}Ar$ studies will be published at a later date.

2. Regional Geology

The Usagaran Orogen of central Tanzania is a Palaeoproterozoic orogenic belt that lies directly east of the ~2.7 Ma Tanzanian Craton (Fig. 1). In the south, the 2.0 Ga Usagaran Orogen links with a similar sequence of rocks of the Ubendian Orogen of western Tanzania. These two orogens are considered by some to be equivalent (Meinhold, 1970; Wendt et al., 1972; Gabert and Wendt, 1974; Priem et al., 1979). However, more recent geochronological information suggests metamorphism in the Ubendian Orogen may be younger (1.95-1.85 Ga) (Lenoir et al., 1994). To the east and north the Usagaran Orogen becomes progressively reworked in the East African Orogen; a zone of Neoproterozoic (620-690 Ma, Möller et al., 2000; Muhongo et al., 2001) orogenesis associated with the collision of East and West Gondwana (Stern, 1994; Dalziel, 1997).

The Usagaran Orogen can be subdivided into two major litho-tectonic units; the Isimani Suite and the Konse Group (Fig. 2). The Isimani Suite, previously referred to as the "Usagaran highly metamorphic rocks" (Whittingham, 1959; Harpum, 1970), lies to the east of the Konse Group and is a zone of high-grade amphibolite, granulite and eclogite facies rocks. Previous workers have subdivided the Isimani Suite into three "lithodeme" named after their type localities (Mruma, 1989), which correlate with the "gneiss-amphibolite series" and the "amphibolite-free gneiss series" of Whittingham (1959) and Meinhold (1970). In detail the Isimani Suite comprises numerous different lithologies. These record a range of different metamorphic assemblages that in part reflect variable degrees of retrograde overprinting, but may also reflect variations in metamorphic conditions throughout the suite. Peak eclogite facies conditions have been constrained at ~750°C and *c.*18 kbar (Möller et al., 1995), while similar age granulite facies metamorphism also in the Isimani Suite took place at 780°C and 10 kbar (Mruma, 1989). An extensive amphibolite facies metamorphism that overprints these high pressure events has yielded pressure-temperature estimates of 4-6 kbar and 500-700°C (Mruma, 1989).

In the past, Usagaran gneisses have been interpreted to have a sedimentary origin due to their lateral extent and the presence of kyanite-bearing mica schists (Mruma, 1989). Mafic rock types have been inferred to be of magmatic origin (Mruma, 1989) and trace and rare-earth

element geochemistry have been used to infer a MORB-type protolith for these rocks (Möller et al., 1995).

The Konse Group (Meinhold, 1970; Mruma, 1989), formerly the Konse Series (Whittingham, 1959; Harpum, 1970), is composed of a stratigraphic succession of seven sedimentary and volcanic formations subsequently metamorphosed at greenschist facies conditions. At its base, the Konse Group unconformably overlies foliated rocks of both the Isimani Suite and the Tanzanian Craton (Whittingham, 1959; Mruma, 1989).

The deformation history of the Usagaran Orogen is complex. However, very little detailed structural work has been undertaken and no previous studies have considered the kinematic evolution of the Usagaran Orogen. Mruma (1989), building on the work of Meinhold (1970), outlined a three-phase deformation history for the Isimani Suite based on foliation and fold relationships. He outlined a first deformation event (D_1) that occurred at high pressure conditions. Eclogite and granulite facies mineral assemblages were considered to have developed at this stage. The latter two deformation events were also thought to have affected the Konse Group. The first of these (D_2/D_{K1} of Mruma, 1989) took place at upper greenschist / lower amphibolite facies conditions and was considered to be the main phase of deformation within the Usagaran Orogen. This deformation was considered to reflect thrusting of the Usagaran Orogen onto the Tanzanian craton. Subsequent D_3/D_{K2} deformation involved minor folding and faulting associated with NE-SW compression (Mruma, 1989).

Previous geochronological constraints on the timing of protolith formation, deformation and metamorphism within the Usagaran Orogen have highlighted the antiquity of the Usagaran protoliths and the importance of Palaeoproterozoic high-grade metamorphism. Depleted mantle Nd model ages of 2.7-3.1 Ga obtained from Usagaran gneisses (Möller et al., 1998) and 2.1-2.5 Ga from post-tectonic granites (Maboko and Nakamura, 1996) suggest that a significant component of Archaean material is common throughout eastern Tanzania. Coupled thermo-barometric analysis and U-Pb monazite data indicate that eclogite facies (M_1) metamorphism took place at 2000±1 Ma ago (Möller et al., 1995). The Konse Group has been dated by correlation with the Ndembera volcano-sedimentary group of Tanzania (Fig. 2, Whittingham, 1959; Mruma, 1989) from which whole rock Rb-Sr data yielded an age of 1895±27 Ma (age recalculated from Wendt et al., 1972, using the decay constant of Steiger

and Jager; 1977). Rb/Sr biotite-whole rock isochrons on the Usagaran gneisses and post-tectonic granites range in age from 432±5 Ma to 1956±53 Ma (recalculated from Wendt et al., 1972) and K-Ar biotite ages range from c. 500-3200 Ma (Wendt et al., 1972; Gabert and Wendt, 1974). Gabert and Wendt (1974) noted that within this range there was a general southeastward younging in ages away from the Tanzanian craton, which they interpreted as resetting by a late Neoproterozoic thermal event associated with the East African Orogen. Discordant U-Pb rutile ages from retrogressed eclogites-facies rocks with a lower intercept of 501±26 Ma support the presence of a Neoproterozoic thermal overprint (Möller et al., 1995).

3. Rock types of the Isimani Suite

The Isimani Suite comprises highly metamorphosed and deformed gneisses. The gneisses are dominated by amphibolite facies mineral assemblages but locally granulite and eclogite facies rocks are preserved. Greenschist facies mineral assemblages locally overprint higher grade metamorphic assemblages. A detailed description of the rock types and metamorphic assemblages found in the Great Ruaha River section is given by Mruma (1989).

We have distinguished two main lithological units in the river section; leucocratic gneiss and mafic amphibolites. All of the rocks contain a strongly developed tectonic foliation (see section 4). The leucocratic gneiss forms the most abundant rock association in the river section and was referred to as the Mbunga River Lithodeme by Mruma (1989). The gneiss is compositionally banded at a range of scales (cm – 100's of metres) (Fig. 3a, d, f, g) and in detail comprises a number of different rock types with varying modal amounts of feldspar, quartz, amphibole and biotite. Amphibolite boudins occur within the leucocratic gneiss and are interpreted as deformed dykes. Throughout the suite, leucocratic gneiss is typically coarse grained and often contains large (2-4 cm diameter) euhedral porphyroclasts of K-feldspar or quartz. In low strain areas the K-feldspar porphyroclasts are euhedral to subhedral and are interpreted as deformed phenocrysts that originated within porphyritic igneous protoliths rather than as porphyroblasts that grew during metamorphism (Vernon and Williams, 1988). Also within these low strain areas some of the compositional variation is clearly related to in-situ melting and the segregation of leucocratic material. Thin bands of amphibolite and quartzo-feldspathic material that are now largely sub-parallel to the main tectonic foliation cut earlier layers and show igneous cross-cutting relationships.

A large area of amphibolites is found in the east of the studied river section (Figs. 2 & 4). Referred to as the Luhomero Lithodeme by Mruma (1989), this unit comprises coarse-grained garnet amphibolite that is both compositionally banded and strongly foliated (Fig. 3c). Compositional layering is commonly delineated by modal variations in garnet, amphibole and plagioclase. However more leucocratic layers also contain quartz. In places, diopside-bearing granulites related to the earliest phase of metamorphism are preserved in this unit, while further north this unit traces into Yalumba Hill where eclogite-facies metamorphic assemblages are preserved within the overprinting amphibolite facies metamorphism (Mruma, 1989; Möller et al., 1995). Similar, but less garnetiferous, amphibolites are also seen towards the middle of the studied section (Fig. 4).

Volumetrically minor, coarse grained kyanite–garnet gneiss is present and is spatially associated with both major and minor amphibolite units. The mineralogy of these rocks is kyanite, garnet, plagioclase, quartz, biotite, white mica ± staurolite (Mruma, 1989). This assemblage is typical of metamorphism of pelitic rock compositions and suggests that these lithologies were derived from a sedimentary protolith. Leucocratic gneiss and amphibolites that volumetrically dominate the Isimani Suite have also been interpreted to be of sedimentary origin (Meinhold, 1970; Mruma, 1989). However, the uniform nature and preserved igneous textures in low strain zones strongly suggest that these rocks originated as igneous rocks.

4. Structural Geometry and Kinematic Evolution of the Isimani Suite

The structural history of the Isimani Suite can be considered in terms of the development of five principal structural elements. We outline these below in terms of a temporal sequence ($D_{1\text{-}5}$) based on consistent relative age relationships observed in the field. However, some of these principal structural elements record variable geometrical and kinematic complexity. Although we have chosen to broadly divide the structure of the Isimani Suite into five temporal stages, we emphasise that each principal structural element may have developed through a prolonged period of heterogeneous single or multiple phase deformation. The significance of this heterogeneous deformation is addressed in detail in the discussion.

Deformation Stage 1 (D_1)

The first phase of deformation within the Isimani Suite resulted in the development of well-developed compositional banding (S_1) (Fig. 3a). In areas where the D_1 structures are only weakly overprinted by subsequent deformation, for example in D_2 fold hinges, a spaced foliation is sometimes observed parallel to the compositional banding. Compositional banding occurs at the centimetre to metre scale in rocks inferred to have igneous protoliths. The compositional banding and subparallel spaced foliation are therefore interpreted to be tectonic in origin. Note that D_1 is similar to the D_1 of Mruma (1989).

Deformation Stage 2 (D_2)

The second phase of deformation in the Isimani Suite is the ubiquitous development of a strong, mylonitic foliation (S_2), often with well-developed mineral elongation lineation (L_2) defined by amphiboles, biotite and quartz (Fig. 3b,c,d). The S_2 foliation is often axial planar to tight to isoclinal folds (F_2) that affect S_1 compositional banding (Mruma, 1989). No systematic relationship between the orientation of F_2 fold hinges and L_2 mineral elongation lineations has been observed (Fig. 4). In most outcrops, the strong S_2 foliation transposes S_1 so that compositional banding and the mylonitic S_2 foliation are now sub-parallel. Kinematic indicators associated with D_2 are generally well developed, but do show a degree of heterogeneity, therefore, we also recorded a qualitative estimate of our confidence in the observed kinematic structures. δ- and σ- porphyroclasts are the most common kinematic indicators (Fig. 3c,d). Shear-bands are also relatively well-developed but cannot be used in isolation as they cannot always be shown to have developed at the time of D_2 deformation (see section on D_4 below). In places kinematic indicators are ambiguous or poorly developed, despite the good development of S_2 and L_2.

The D_2 deformation observed in the Great Ruaha River section can be subdivided into five distinct structural domains (Fig. 4). These domains record different structural geometry and kinematic orientations but also correlate with major lithological changes in the river section (Fig. 4). In most cases the domains are characterised by internally consistent S_2 and L_2 orientations (Fig. 4). Domain 1 garnet amphibolites in the east of the section, which correlate with eclogite facies rocks further north, record some variability but are dominated by ENE

dipping S_2 foliations and shallowly plunging NNW-SSE oriented L_2 orientations (Fig. 4). Consistent kinematics from this domain indicate top-to-N or top-to-NW shearing (Fig. 5).

To the west, domain 2 has S_2 foliations dipping to the ENE, similar to those in domain 1. However, L_2 has a distinctly different shallow, NE plunging dip-slip orientation (Fig. 4). Well-developed kinematic indicators record a consistent top-to-NE sense of shear throughout this domain (Fig. 5). Similar NE-SW oriented L_2 mineral lineations are seen in domain 3 but they lie on SE-dipping S_2 foliations and therefore indicate apparent strike-slip shearing (Fig. 4). Kinematic indicators in domain 3 record a top-to-NE sense of shear associated with sinistral wrench kinematics (Fig. 5). There is no obvious lithological or structural break observed between domains 2 and 3 and we note a progressive change in orientation of S2 across the domain (Fig. 4). We interpret the difference between these two domains to reflect reorientation of the S_2 foliation by later deformation. This contrasts with the boundary between domains 1 and 2, which although not exposed in the river section, is seen to cut the post-kinematic Kidete Granite (Fig. 2) and is therefore tectonic in nature.

S_2 foliations in domain 4 have a similar orientation to those in domain 3. However, L_2 orientations are orthogonal to those in domain 3, and in domain 4 plunge moderately to the SE (Fig. 4). Although kinematic information is reasonably well developed in the west of domain 4, there are few consistent kinematic indicators developed immediately in the footwall to domain 3 (Fig. 5). Kinematic indicators in the west of domain 4 record a consistent top-to-NW or thrust sense of shear. Similar, but much less well developed shear sense indicators are also present in the easterly section of domain 4. However, top-to-SE kinematic indicators are also present. These ambiguous kinematics may have formed synchronously during D_2 deformation. However, there are also a number of discrete top-to-SE shear zones which probably relate to subsequent deformation (D_4). There is a possibility that some of the ambiguous kinematics in this section of domain 3 are related to the overprinting of two different deformation events. Clearly, there is a significant change in structure between domain 3 and 4. This change corresponds to a complex zone of deformation located at an amphibolite layer, in which S_2 records top-to-NW kinematics (Fig. 5). This zone corresponds to the location of younger, discrete top-to-SE (D_4) shear zone that has an apparent extensional sense.

Domain 5 has similar S_2 and L_2 orientations to domain 4. Domain 5 is kinematically relatively complex and although dominated by top-to-NW shearing, some minor sinistral strike slip deformation associated with sub-horizontal, NE-trending L_2 lineations is apparent. The boundary between domains 4 and 5 is a younger D_4 extensional structure (Figs. 3h and 4).

In a few localities throughout the river section the evolution of D_2 deformation can be inferred by the preservation of lower strain zones in which only early parts of the D_2 deformation path are developed. The lower strain zones mainly occur in strain shadow zones adjacent to competent mafic units. The best example of these occurs mid way along the section (UTM 37M, 018465E, 921022S). Here a mafic igneous unit truncates close folds of the S_1 compositional banding and weak axial planar S_2 fabrics but is itself deformed and wrapped by mylonitic S_2 foliations with associated isoclinal F_2 folds (Fig. 6). The mafic unit itself is boudinaged and contains S_2 foliations at its margins that are parallel to the high strain S_2 foliation in the adjacent gneisses (Fig. 6). We interpret these relationships to indicate syn-deformational intrusion of mafic bodies during progressive D_2 deformation. Similar zones of discrete low and high strain are occasionally observed in the gneisses. In these cases, close folding of the compositional banding has axial planar orientations parallel to adjacent mylonitic S_2 domains (Fig. 3e). Again we interpret this to reflect the preservation of low strain areas, developed within the early stages of the S_2 deformation path, between zones of more intense localised S_2 deformation.

Deformation Stage 3 (D_3)

The S_2 foliation in domains 1 and 2 is locally overprinted by folds related to a third stage of deformation (D_3) (Fig 3a). These folds (F_3) occur on the scale of a few metres and are close, inclined to overturned, NW verging folds with shallowly plunging NE-SW hinges (Fig. 4). The folds affect S_2 and also refold the tight to isoclinal F_2 folds. Axial planar foliations (S_3) are commonly developed during F_3 folding. The metamorphic grade of D_3 fabrics are indistinguishable from those developed during D_2, which may reflect an association with the later stages of D_2. Occasionally pegmatites lie along the axial planes of F_3 structures. Although these are not folded and therefore post-date F_3, there are no relative age relationships between these and subsequent deformation stages. However, it is possible that they intruded at the end of the D_3 deformation event.

Deformation Stage 4 (D_4)

Discrete shear zones that cut S_1 compositional banding and both S_2/S_3 foliations and associated F_2/F_3 folds are seen throughout the Isimani section (Fig. 3f). The offset of compositional banding (S_1) indicates metre-scale dip separations, though rarely could lineations on the shear surface be measured. In most cases these zones have apparent extensional geometries relative to the present day Earth's surface. The shear zones record plastic-brittle characteristics with discrete shear surfaces and reorientation of external foliations parallel to the shear zone. The shear zones also have different styles depending on whether the host lithology is the felsic to intermediate gneiss or the garnet amphibolite.

In the more felsic gneiss the shear zones are discrete and narrow with complex curviplanar geometries (Fig. 3f,g). In any particular area, conjugate geometries are commonly observed (Fig 3g). In a few cases, antithetic minor extensional structures associated with larger synthetic structures, appear geometrically identical to shearbands or extensional crenulation cleavage and cut the S_2 foliation (Fig 3g). The presence of D_4 related structures that look geometrically similar to S_2 shearbands means that shearbands alone cannot be safely used to document the kinematic evolution of D_2 deformation.

Similar shear zones in the garnet amphibolite are associated with the retrogression of garnet and hornblende to a greenschist facies assemblages of actinolite, chlorite and plagioclase. Pseudomorphs after garnet are often deformed immediately adjacent to the shear zone but are undeformed only a few centimetres from the discrete shear surface. This indicates that the zone of retrogression extends beyond the zone of deformation. However, the close spatial relationship between retrogression and deformation suggests that the two processes are linked.

Two outcrop scale extensional structures are exposed in the section. The first occurs at the location of an amphibolite layer in the section and is close to the D_2 domain boundary of domains 3 and 4. The zone is a metre-wide zone of top-to-SE extensional shear that overprints a well-developed S_2 foliation associated with weak top-to-NW kinematics. In the footwall to this structure (top of domain 4) smaller scale top-to-SE structures are also present that may also be related to D_4 deformation. The second extensional structure occurs towards the western end of the section where it reactivates the earlier S_2 foliation. Kinematics in this

shear zone are again top-to-SE, indicating an apparent extensional displacement (Fig. 3h). In both cases, these zones are characterised by greenschist facies mineral assemblages that are now extensively weathered. Therefore we interpret these two shear zones to postdate the higher grade D_3 deformation. As the metamorphism and kinematics associated with the two shear zones are similar to the smaller scale extensional (D_4) structures, we have bracketed all of these structures together as D_4. However, we note that the lack of interaction of smaller and larger scale features means that such an assumption may not be valid.

Deformation Stage 5 (D_5)

The contact between the Isimani Suite and the Konse Group can be seen in a single continuous outcrop in the river section (Fig. 4, 5) and is marked by a series of different fault rock types that overprint originally different rock types. Fault rock types associated with the contact include gouge, cataclasite and phyllonite. Amphibolites within the original Isimani sequence now comprise chlorite and actinolite, which are strongly foliated and contain ubiquitous shear-bands indicating top-to-NW shearing. Quartzo-feldspathic rocks from the Isimani Suite are characterised by quartz and sericite and are again strongly deformed. These mineral assemblages indicate dynamic recrystallisation during thrusting of the Isimani Suite over the Konse Group at greenschist facies conditions.

Similar greenschist facies retrogression is seen in the garnet amphibolites up to 100m from the contact. Close to the contact, garnets are completely replaced by plagioclase and actinolite and the resulting pseudomorphs are variably, but sometimes strongly, deformed. Finite ellipticities (R_f) of pseudomorphs reach as much as 25:1 on XY planes and appear to be related to strongly constrictional strains. In other cases, both XZ and YZ sections show flattening (R_f = 3.4 and 1.7 respectively) consistent with oblate strains. This deformation and retrogression is spatially related to the contact and is thus inferred to be related to thrusting of the Isimani Suite over the Konse Group.

The similar metamorphic grades and absence of overprinting relationships between D_4 and D_5 structures makes the relative ages of D_4 and D_5 difficult to assess and it is possible that D_5 developed synchronously with some of the D_4 structures.

6. Zircon U-Th-Pb Geochronology

U, Th and Pb isotope measurements from zircons from a leucocratic gneiss of the Isimani Suite and the post-tectonic Kidete Granite were measured to determine igneous crystallisation ages and constrain the age of amphibolite-grade deformation in the Isimani Suite.

Analytical Techniques

Zircons were separated from crushed rock samples by conventional magnetic and methylene iodide liquid separation. Grains were handpicked and mounted in epoxy resin discs that were coated with a thin membrane of gold that produced a resistivity of 10-20 ohms across the disc. The mounts were then imaged under cathodoluminescence (CL). The resulting images (Fig. 7) highlight distortions in the crystal lattice (Stevens Kalceff et al., 2000) that are related to trace-element distribution and/or radiation damage (e.g. Rubatto and Gebauer, 2000).

Zircon U-Th-Pb isotopic data was collected using the Sensitive High Resolution Ion Microprobe Mass Spectrometer (SHRIMP II) based in the John de Laeter Centre of Mass Spectrometry, Perth, Western Australia. The sensitivity for Pb isotopes in zircon using SHRIMP II was ~18 cps/ppm/nA, the primary beam current was 2.5-3.0 nA and mass resolution was ~5000. Correction of measured isotopic ratios for common Pb was based on the measured ^{204}Pb in each sample and often represented a <1% correction to the ^{206}Pb counts (see %common ^{206}Pb in Table 1). The common Pb component, being largely surface contaminant, was modelled on the composition of Broken Hill ore Pb.

Pb/U isotopic ratios were corrected for instrumental inter-element discrimination using the observed covariation between Pb^+/U^+ and UO^+/U^+ (Hinthorne et al., 1979; Compston et al., 1984) determined from interspersed analyses of the Perth standard zircon CZ3. CZ3 is a single zircon megacryst from Sri Lanka with an age of 564 Ma and a $^{206}Pb/^{238}U$=0.0914 (Nelson, 1997).

Sample and Zircon Characteristics

T01-01 (UTM 37S, 0181224E, 9209045S) is an undeformed two feldspar granite belonging to the Kidete granite (Fig. 2). This granite cuts the pervasive S_2 fabric of the Isimani felsic gneiss but the relationship of the granite to spatially localised deformations (D_{3-5}) is unclear. Zircons separated from the Kidete granite are between 100-300 μm long and can be subdivided into three types based on morphology and CL response (Fig. 7a,b,c & Table 1).

Type 1 zircons are euhedral elongate prisms (3-4:1 aspect ratio) which show thin oscillatory zoning under CL and an overall light to dark core to rim transition (Fig. 7a). Type 2 zircons are subhedral to anhedral and have sub-circular to elliptical cross-sections. Most have a distinct thin highly luminescent rim of zircon (Fig. 7b). Occasional euhedral dark zircon overgrowths partially surround the grain. Type 3 zircons are complex grains some of which contain distinct zoned cores, a succession of zones rimming the core and occasionally, thin brightly luminescent (Fig. 7c) and broken grains.

T01-24b (UTM 37S, 0182867E, 9210506S) is a granitic gneiss with a pronounced S_2 foliation and L_2 mineral elongation lineation from the Isimani Suite in the Great Ruaha river valley. Zircons separated from this sample are between 100-400 μm long, subhedral to euhedral grains with a generally light to dark core to rim CL response. Discrete oscillatory-zoned rims occur in some grains and a extremely thin brightly luminescent rims partially surround a number of grains (Fig. 7d). These bright rims were too thin to analyse.

U-Th-Pb SHRIMP Results

Results of U and Pb isotope analysis of zircons from T01-01 largely plot along two discordia lines on a concordia diagram (Table 1; Fig. 8a). The younger of these discordia lines has upper and lower concordia intercepts at 1877 ± 7 and 42 ± 54 Ma respectively (MSWD = 1.7). All analyses that lie on this discordia are from Type 1 zircons (see below). The euhedral form of these grains, oscillatory-banding under CL and the young age of the zircons suggest that the upper intercept age of 1877 ± 7 Ma represents the crystallisation of this post-tectonic granite. The older discordia is less well constrained with upper and lower concordia intercepts of 2698 ± 15 and 200 ± 230 Ma respectively (MSWD = 5.1). Type 2 zircons make up most of these analyses with two analyses from the cores of type 1 grains. The upper intercept of this discordia is identical (within error) to the crystallisation age of the population of zircons in sample T01-24b (see below) and therefore these grains are interpreted as locally derived xenocrysts from the Isimani gneiss. Two older grains include a core analysis from a complex Type 3 grain (Fig. 7c) that is rimmed by zircon with a $^{207}Pb/^{206}Pb$ age close to the upper intercept of the older discordia (Table 1). These grains are interpreted as second-order xenocrysts, first incorporated into the Isimani gneiss protolith, then scavenged again in the Kidete intrusion.

Zircons from T01-24b all have pre-2.2 Ga $^{207}Pb/^{206}Pb$ ages (Table 1). Twenty analyses define a discordia line with upper and lower concordia intercepts at 2705 ± 11 and 172 ± 43 Ma respectively (MSWD = 10.5) (Fig. 8b). Point selected for inclusion in the discordia were chosen by eye and are indistinguishable in form or luminescence from other analysis spots that lie off the discordia. The broadly euhedral form and oscillatory zoned CL response suggests that the upper intercept of 2705 ± 11 Ma represents crystallisation from a granitic magma. The relatively high MSWD reflects a 60 Ma spread in concordant $^{207}Pb/^{206}Pb$ ages between ~2670 and 2730 Ma (Fig. 8b inset) that suggests either one extended period of zircon growth, or a number of individual growth periods unresolvable by the SHRIMP method. Four concordant and discordant analyses have $^{207}Pb/^{235}U$ ages older than 2730 Ma. These are interpreted as xenocrysts in the 2705 ± 11 Ma granite. In addition, a number of grains have $^{207}Pb/^{235}U$ ratios that result in them plotting left of the discordia line with $^{207}Pb/^{206}Pb$ ages between ~2400 to 2660 Ma (Fig. 8b). This large age range could indicate either: 1) a sedimentary protolith, this interpretation is discounted here by the extensive, uniform lithology of the outcrop and the preservation of igneous feldspar phenocrysts in low-strain zones; 2) diverse and populous xenocrysts in a ~2400 Ma intrusion, an unlikely scenario considering the scarcity of the younger zircons; or 3) the structural imbricating of minor amounts of younger granitic material within this mylonitic gneiss.

The results of the U-Pb SHRIMP study of these two samples from the Usagaran orogen constrain the pervasive, high-strain ductile deformation in the Isimani Suite to between at least 2705 ± 11 and 1877 ± 7 Ma. In addition, the similarity in age between the protolith of the Isimani granite gneiss and the xenocrysts in the post-tectonic Kidete granite (samples from ~2 km apart) suggest that much of the felsic component of the Isimani Suite is ~2.7 Ga, considerably older than the ~2.0 Ga eclogite-facies metamorphism but similar to crustal-residence ages (O'Nions et al., 1983) reported for the Isimani Suite based on Nd isotopic date (Möller et al., 1998).

7. Discussion

Structural Evolution of the Isimani Suite

The Isimani Suite of the Usagaran Orogen records a complex structural history, which we have subdivided into five ‘events’. The first phase of deformation resulted in the formation of a planar compositional fabric and subparallel foliation (S_1). S_1 is strongly overprinted by a

second D_2 deformation, which is the major deformation phase to affect the Isimani in this area. The D_2 stage of deformation resulted in the extensive reorientation of D_1 features and the formation of a composite S_1/S_2 foliation. D_2 deformation was an extensive high strain deformation that resulted in the formation of mylonitic rocks throughout all of the section we have studied. S_2 foliations commonly have aligned euhedral amphiboles, suggesting that this deformation took place at amphibolite facies metamorphic grades. In a few zones of low strain evidence is preserved for syn-D_2 intrusion of mafic dykes and *in situ* melting of the leucocratic gneisses during the early stages of D_2. The amphibolite grade metamorphism that is dominant within the Isimani Suite of rocks overprints higher grade granulite and eclogite facies metamorphism, evidence for which is only locally preserved. This observation is consistent with the interpretation of Mruma (1989) that the high pressure metamorphism formed during the earliest stage of Isimani deformation (D_1 of this study).

Foliation (S_2), lineation (L_2) and shear sense indicators associated with D_2 show a marked variation that enable the recognition of 5 structural domains. These domains represent packages of rocks that have different D_2 principal stretch orientations and/or record different senses of shear. In some cases, for example between domains 2 and 3, the variation appears to be the result of a subsequent reorientation of the S_2 foliation (Fig. 5). However, in most cases the relationship between these different domains is not so clear and is often masked by later localised deformation at greenschist facies conditions (D_4 and D_5). These features indicate strain localisation or partitioning within the evolving high strain zone that can be explained by three end-member models. We suggest that a component of each of these end-members is responsible in the structural evolution of the Isimani Suite (Fig. 9).

Model 1: General Shear

General shear (e.g. transpression) can lead to considerable geometric and kinematic complexity in high strain zones (Harland, 1971), especially when the pure and simple shear components of the general shear deformation are partitioned with respect to space and time (Dewey et al., 1998). As a result, discrete zones with differing S_2/L_2 geometries may develop in zones deforming at the same time. In a high strain zone where the convergence angle of the blocks either side of the deforming zone are <20° and there is no strain localisation, the differential accommodation of pure and simple shear strain components may lead to the formation of a mineral lineation that may then progressively diminish and begin to form in a

new orientation (Tikoff and Greene, 1997; Fossen and Tikoff, 1998). As a result, mineral elongation direction may change direction (through 90°) and intensity with increasing strain, while recording consistent shear sense throughout the deformation.

If strain is localised into discrete zones accommodating different amounts of pure and simple shear, zones accommodating pure shear deformation must stretch parallel to the high strain zone margin and differential stretching of pure and simple shear domains must be accommodated (e.g. Dewey et al, 1998). In such a model, we would expect to see discrete zones dominated by simple shear and consistent kinematic indicators interspersed with domains with orthorhombic symmetries and no discernable shear sense. This is seen in the studied section, with zones of ambiguous kinematics (top of domain 4) adjacent to domains with a consistent shear sense (domain 3) (Fig 9). In this model, different lineation orientations could develop in the different domains depending on the degree and orientation of stretch within the pure and simple shear domains. If pure shear maximum stretch were parallel to the shear direction in adjacent domains then a constant lineation direction would be seen in the different high strain domains. Orthogonal lineation orientations would be seen if pure shear stretch was perpendicular to the shear direction.

In the domains studied here, there are systematic variations in the orientation of L_2 throughout the section. However, the orientation of L_2 on the S_2 foliation surface always appears to be parallel to the shear direction that can be inferred by the monoclinic symmetry of kinematic indicators (Fig. 9). We have been unable to demonstrate any situations where the shear direction was oriented at angles strongly oblique to L_2. Therefore, we cannot argue that the variation in lineation orientations we see are related to the localisation of pure and simple shear components of a general shear deformation. The different orientations of L_2 in the different domains correlate with differing simple shear directions in these different domains. To explain our observations by a general shear model requires there to be partitioning of the deformation into at least two non-coaxial zones of deformation which have kinematic orientations that are currently both strike-parallel (top-to-NE) and highly oblique (top-to-NW) to the orogen (Fig. 9). The partitioning of deformation into contemporaneous strike-parallel and strike-normal motions in obliquely convergent orogens is recognised from field studies (Suarez et al., 1983; Mount and Suppe, 1992), is predicted on theoretical grounds (Molnar, 1992; Platt, 1993b) and has been shown by experiment (Richard and Cobbold, 1990; Braun

and Beaumont, 1995). As a consequence, such partitioning is often used as evidence for transpressional orogenesis.

Model 2: Reworking during a Single Progressive Deformation

The second model requires that high strain structures developed in the early stages of the D_2 deformation path are subsequently overprinted by younger stages of D_2 deformation. The distribution of domains with different D_2 geometry and kinematics requires the younger deformation to be localised. The evidence from strain shadows around small mafic bodies (Fig. 6) indicates that the D_2 deformation developed progressively and became more intense with time. However, all D_2 foliations appear to have developed at amphibolite grade and there was no significant change in metamorphic mineralogy during the time period over which D_2 took place. Consistent overprinting relationships between D_2 and other structures also indicate the same relative age framework for D_2 deformation throughout the section. Yet these observations are insufficient criteria to discount a temporal and spatial variation of changing D_2 strain throughout the domainal structure of the studied section. Geochronological data from single high strain zones clearly indicate that deformation can migrate spatially over time and that the kinematics of the deformation can also change during progressive deformation (Reddy et al., 1999). At this stage, the geochronological data that could support this model do not exist. Although we argue that this type of reworking is important we are currently unable to assess the possibility of reworking of early D_2 structural elements by younger D_2 elements formed under similar pressure and temperature conditions.

Model 3: Reactivation

A third model that may explain the different D_2 structural orientation between domains is one in which the domains are juxtaposed by narrow zones of younger deformation which reactivate the older D_2 structure. The boundary between domains 4 & 5 is marked by a greenschist facies extensional shear zone that has a different kinematic sense to adjacent amphibolite facies rocks and must have developed after D_2 structures. The contact between domains 1 & 2 was not exposed in the section studied here. However, Mruma (1989) reports that the contact between domains 1 and 2 is tectonic in origin and regional mapping (Fig. 2) indicates that this contact cuts the 1877 ± 7 Ma Kidete Granite (Figs. 2 & 9). Many domain contacts are therefore demonstrably zones of younger localised strain that post-date D_2 (Fig. 9). The variable geometry and kinematics of the D_2 deformation may therefore reflect juxtaposition by later deformation. This could explain the orogen oblique kinematics

preserved in domain 1, but seems unlikely to account for the difference between domains 2 and 3, or between domains 3 and 4 where a 90° rotation around a rotation axis perpendicular to the D_4 structure would be required. Although possible, we see no evidence to support such a large rotation.

In summary, we conclude that D_2 records a complex geometric and kinematic evolution. In part this reflects modification by later greenschist facies structures (Fig. 9). However, it is also possible that spatial and temporal strain localisation during general shear and the reworking of early formed D_2 structures by later parts of the D_2 deformation path (Fig. 9) played a significant role in the domainal structure of D_2 deformation. Therefore, the data are broadly consistent with the D_2 kinematic domains developing during progressive deformation within an obliquely convergent sinistral transpressional system (Fig. 9) subsequently reworked and reactivated at greenschist facies conditions (D_4 and D_5). The timing of D_2 deformation is poorly constrained to between 2705 ± 11 Ma and 1877 ± 7 Ma by U-Pb SHRIMP analysis of a pre-D_2 protolith and a post-D_2 granite. However, eclogite-facies metamorphism has been dated at 2000 ± 1 Ma (Möller et al., 1995). Since this metamorphism is associated with D_1 deformation, D_2 deformation, and oblique convergence, took place between 2001 and 1870 Ma.

The spatially restricted F_3 folds post-date D_2 deformation but formed at similar metamorphic conditions. The NW-verging geometry of the folds, combined with the metamorphic grade similarity may indicate that the D_3 deformation represents the later stages of the deformation path associated with the top-to-N D_2 shearing. However, such a model cannot be proven by the existing data.

D_4 and D_5 greenschist facies shear zones cut earlier structural features and record different metamorphic conditions than D_1-D_3 structures. A greenschist-facies D_5 fault thrusts the Isimani Suite over the Konse Group along the Great Ruaha river section (Fig. 5). However, to the south of this section, the Konse Group was mapped as unconformably overlying the Isimani Suite (Whittingham, 1959). This relationship was disputed by Meinhold (1970), who interpreted the Konse and Isimani and time-equivalent units differentiated only by metamorphic facies. However, detailed mapping by Mruma (1989) detailed the lithological differences between the Konse Group and any possible protolith of the Isimani Suite and

recorded a well preserved unconformity between the two. An unconformable relationship between the Konse Group and the Isimani Suite indicates that the Isimani Suite has a complex thermal history. Firstly, the Isimani Suite must have passed through a retrograde greenschist facies metamorphism while being exhumed prior to Konse Group deposition. Then the Isimani Suite and the Konse Group must have been buried and metamorphosed at greenschist facies, before the Isimani Suite was thrust over the Konse Group during D_5 shearing and subsequently the whole package was exhumed.

Within this framework it is difficult to assess the relative timing and tectonic significance of the D_4 extensional shear zones and associated greenschist facies metamorphic conditions. Greenschist facies conditions may be related to retrograde metamorphism associated with initial exhumation of the Isimani rocks. In this case we would expect Palaeoproterozoic deformation ages, otherwise eclogite facies mineral assemblages would not be preserved. Alternatively, the deformation may be related to the second stage of greenschist facies metamorphism and may have occurred synchronously with D_5 thrusting. The age of this second greenschist facies event, responsible for the peak metamorphic conditions in the Konse Group, is currently unknown. Mruma (1989) correlated the main structure (D_1) in the Konse Group with the Isimani Suite deformation we refer to as D_2 and therefore inferred that the greenschist facies Konse Group metamorphism was Palaeoproterozoic in age. This correlation is based on structural geometry and ignores the difference in metamorphic grade. Our data from the Isimani Suite indicate that D_2 and D_4 structures are broadly subparallel and therefore that the coincidence of structural geometry can not be used as evidence that the structures developed contemporaneously. K-Ar biotite ages and Rb-Sr biotite-whole rock isochrons from the Usagaran Orogen (Wendt et al., 1972) have also been used to argue that greenschist facies metamorphism in the Konse Group was of Palaeoproterozoic age (Gabert, 1973; Gabert and Wendt, 1974). However, the two published Rb-Sr ages from the Ruaha river section (Wendt et al., 1972) recalculated using presently accepted decay constants produce ages of 1803 ± 25 Ma and 432 ± 5 Ma. K-Ar data are unable to discriminate the presence of excess ^{40}Ar and metamorphic biotite commonly contains an excess ^{40}Ar component (Roddick et al., 1980). Because of the uncertainty in both the Rb-Sr biotite-whole rock and K-Ar techniques it is possible that the age of greenschist facies metamorphism in the study region could be much younger than the reported Palaeoproterozoic ages. Indeed, it is possible that the greenschist facies metamorphism is related to the East African Orogen, a suggestion

supported by the lower intercept of a multi-phase U-Th-Pb discordia line from the Isimani gneisses of 501 ± 26 Ma (Möller et al., 1995). Currently, there are no structural criteria available to discriminate between these two possibilities but ongoing geochronological work will address these issues further.

Implications for the Tectonic Evolution of the Usagaran Orogen

U-Pb zircon data from an Isimanian leucocratic gneiss and presumed Isimanian xenocrysts in a later intrusion both yield concordant ages that indicate Archaean crystallisation of the original protoliths at *c.* 2.7 Ga.. This age lies within the range of published Usagaran and Tanzanian craton Nd model ages (Ben Othman et al., 1984; Maboko, 1995; Maboko and Nakamura, 1996; Möller et al., 1998; Maboko, 2000) and confirms that the Usagaran Orogen comprises reworked Archaean material of similar age as the Tanzanian craton. Similar rock types, with similar mylonitic foliations, similar Nd model ages and high pressure mineral assemblages, can be traced for at least 50 km to the east of the region studied here. In addition, gneisses exposed 150 km to the east in the Uluguru mountains (Fig. 1) contain 2.7 Ga zircons interpreted to reflect the protolith intrusion age (Muhongo et al., 2001) and preserve Nd and Pb isotopic values consistent with Archaean crust reworked in Proterozoic times (Maboko, 1995; Möller et al., 1995; Stern, 2002). The area to the east of the Tanzanian Craton therefore comprises a large volume of Archaean material formed around 2.7 Ga ago and subsequently reworked in the Palaeoproterozoic Usagaran and Neoproterozoic East African orogens.

Eclogite facies metamorphism of MORB-like mafic rocks preserved in the Isimani Suite of the Usagaran Orogen has been interpreted to reflect the subduction of ~2.0 Ga oceanic crust (Möller et al., 1995). Thermobarometrical and geochronological data from elsewhere in the Usagaran Orogen, and from the contiguous Ubendian Orogen, have been interpreted to reflect SE-dipping subduction along an Andean-type convergent margin at this time (Ring et al., 1997). In the northern Usagaran Orogen, garnet amphibolite rocks that represent retrogressed eclogites form a number of slab-like bodies that are completely surrounded by mineralogically homogenous leucocratic gneisses that crystallised at ~2.7 Ga. The observed association in the Isimani Suite of mafic gneiss, metapelite and voluminous granitoid gneiss of uniform age is not one that would be expected in an intra-ocean or ocean-margin subduction/accretion complex where exotic material of diverse origin, rock type and age are

accreted and juxtaposed. Instead three models are proposed to explain the observed rock associations in the northern Usagaran Orogen. 1) Supra-subduction zone accretion of voluminous uniform-aged granitoid, partially subducted slices of MOR-like basalt and mudrocks. 2) Thinning of the eastern Tanzanian craton followed by partial subduction of the margin and subsequent exhumation. 3) Rifting of the eastern Tanzanian craton followed by subduction and closure of the marginal basin and continued accretion of the ribbon continent onto the craton.

In the first model, the uniform crystallisation age of the granitoids east of, west of, and within the subduction complex suggests a fortuitous amalgamation of continental material that originated in diverse locations. This scenario seems unlikely to us. The second model requires the extrusion of MOR-like basalt onto the margin of the Tanzanian Craton prior to subduction. Extrusion of MOR-like basalt is required to explain the close spatial relationship between mafic rocks and metasedimentary kyanite-garnet gneiss. The third model differs from the second in that marginal basin crust is developed during a phase of pre-contraction rifting on the craton margin. We envisage that subduction was restricted to the consumption of marginal basin crust (represented by the mafic amphibolites) that separated continental material of similar origin. The ribbon continent outboard of the marginal basin was then accreted onto the margin of the craton by sinistral transpression after the subduction of the marginal basin. Continuing subduction may then have continued outboard of this collisional zone providing a source for the voluminous post-tectonic magmatism seen throughout the Usagaran orogen. At this stage, this is our preferred model.

All of these models differ from tectonic scenarios previously suggested for the region in positioning the Usagaran Orogen in a continental margin setting. In our models, the MORB-type mafic rocks do not represent true oceanic crust but MORB formed in a continental margin environment. Existing geochemical data does not allow discrimination between these alternative models for the origin of the MORB-type protoliths.

The structural history preserved in the Isimani Suite is dominated by post-subduction deformation that reveals little of the tectonic environment during subduction. D_2 deformation and associated amphibolite facies metamorphism represent sinistral transpression associated with oblique convergence across the Usagaran Orogen. The geometry and kinematics of

orogen–perpendicular D_2 structures indicates a thrust sense of displacement of Usagaran rocks onto the Tanzanian craton in the west. We interpret this to represent migration of the Isimani Suite towards the foreland of the orogen; a model consistent with SE-dipping subduction prior to collision. The voluminous post-tectonic granitic intrusions within the Tanzania Craton and the Usagaran orogen (including the Kidete granite) may indicate a switch in subduction polarity with continuing subduction after closure of the Usagaran marginal basin dipping west beneath the then amalgamated Tanzania Craton/Usagaran orogen.

8. Conclusions

High strain amphibolite-facies deformation in the Isimani Suite of the Usagaran Orogen, Tanzania, is characterised by variable foliation, lineation and kinematic orientations, which are consistent with formation by sinistral transpression during oblique convergence. This deformation (D_2) post-dates the formation of eclogite facies rocks that are locally preserved within the Usagaran Orogen and may be related to exhumation of the high pressure rocks. Geochronological data, including new zircon SHRIMP data, indicate that this deformation took place between 1.87 – 2.0 Ga. Greenschist facies deformation (D_4 and D_5) overprints the dominant D_2 strain and reflects localised reactivation of early structures. The ages of these D_4 and D_5 deformation phases are poorly constrained and may reflect deformation during Palaeoproterozoic exhumation of the Usagaran Orogen or during the late Neoproterozoic East African orogeny. Existing tectonic models, based on metamorphic and geochemical arguments do not adequately explain the formation and exhumation of eclogite facies rocks in the Usagaran Orogen and we suggest that the eclogites formed during subduction of the stretched or rifted continental margin of the Tanzanian craton and were exhumed during transpression associated with sinistral oblique convergence.

Acknowledgements

We dedicate this paper to Chris Powell for inspiring us to work on Palaeoproterozoic geology. This research was supported by the Australian Research Council by small and large Discovery grants to SMR and ASC. Fieldwork in Tanzania was facilitated by a number of people, but we especially thank Rev. Fr. Camillus Fillo Mitti of Rudi Parrish for his generous hospitality. The zircon analyses were carried out on the Sensitive High-mass Resolution Ion Microprobe mass spectrometer (SHRIMP II) operated by a consortium consisting of Curtin

University of Technology, the Geological Survey of Western Australia, and the University of Western Australia with the support of the Australian Research Council. We appreciate the assistance of Peter Kinny, Sasha Nemchin and Allen Kennedy during SHRIMP analysis and data reduction. Ken Ludwig is thanked for providing copies of his programs "Squid" and Isoplot" that were invaluable for data reduction. Thorough and constructive reviews by Andreas Möller, Kevin Ansdell and Tom Blenkinsop significantly improved this manuscript and are greatly appreciated. This paper is Tectonic Special Research Centre contribution n^{o}. 202.

References

Barnicoat, A.C. and Fry, N., 1986. High-pressure metamorphism of the Zermatt-Saas ophiolite zone, Switzerland. Journal of the Geological Society, 143: 607-618.

Ben Othman, D., Polvé, M. and Allègre, C.J., 1984. Nd-Sr isotopic composition of granulites and constraints on the evolution of the lower continental crust. Nature, 307: 510-515.

Braun, J. and Beaumont, C., 1995. Three-dimensional numerical experiments of strain partitioning at oblique plate boundaries: implications for contrasting tectonic styles in the southern Coast Ranges, California and central South Island, New Zealand. Journal of Geophysical Research-Solid Earth, 100: 18059-18074.

Compston, W., Williams, I.S. and Meyer, C., 1984. U-Pb geochronology of zircons from lunar breccia 73217 using a sensitive high mass-resolution ion microprobe. Journal of Geophysical Research, 89(Supplement): B525-B534.

Dalziel, I.W.D., 1997. Neoproterozoic-Paleozoic geography and tectonics: Review, hypothesis, environmental speculation. Geological Society of America Bulletin, 109: 16-42.

De Roever, W., 1956. Some differences between post-Paleozoic and older regional metamorphism. Geologie en Mijnbouw, 18: 123-127.

Dewey, J.F., Holdsworth, R.E. and Strachan, R.A., 1998. Transpression and transtension zones. In: H. R.E., R.A. Strachan and J.F. Dewey (Editors), Continental Transpressional and Transtensional Tectonics, 135. Geological Society, London, Special Publication, pp. 1-14.

Ernst, W.G., 1971. Metamorphic zonations on presumably subducted lithospheric plates from Japan, California and the Alps. Contributions to Mineralogy and Petrology, 34: 43-59.

Fossen, H. and Tikoff, B., 1998. Extended models of transpresson and transtension, and application to tectonic settings. In: H. R.E., R.A. Strachan and J.F. Dewey (Editors), Continental Transpressional and Transtensional Tectonics, 135. Geological Society, London, Special Publication, pp. 15-33.

Gabert, G., 1973. Über granitische Gesteine des Dodoman und Usagaran im südlichen Hochland von Tanzania (Ostafrica). Geologisches Jahrbuch, B6: 3-50.

Gabert, G. and Wendt, I., 1974. Datierung von granitischen Gesteinen im Dodoman- und Usagaran-System und in der Ndembera-Serie (Tanzania). Geologisches Jahrbuch, B11: 3-55.

Harland, W.B., 1971. Tectonic transpression in Caledonian Spitzbergen. Geological Magazine, 108: 27-42.

Harpum, J.R., 1970. Summary of the Geology of Tanzania, Part V: Structure and Geotectonics of the Precambrian, Memoir 1. Mineral Resources Division, Government of Tanzania, Dodoma, 58 pp.

Hinthorne, J.R., Anderson, C.A., Conrad, R.L. and Lovering, J.F., 1979. Single-grain 207Pb/206Pb and U/Pb age determinations with a 10 μm spatial resolution using the ion microprobe mass analyser (IMMA). Chemical Geology, 25: 271-303.

Lenoir, J.-L. et al., 1994. Origin and regional significance of late Precambrian and early Palaeozoic granitoids in the Pan-African belt of Somalia. Geologische Rundschau, 83: 624-641.

Maboko, M.A.H., 1995. Neodymium isotopic constraints on the protolith ages of rocks involved in Pan-African tectonism in the Mozambique Belt of Tanzania. Journal of the Geological Society, London, 152: 911-916.

Maboko, M.A.H., 2000. Nd and Sr isotopic investigation of the Archean-Proterozoic boundary in north eastern Tanzania: constraints on the nature of Neoproterozoic tectonism in the Mozambique Belt. Precambrian Research, 102: 87-98.

Maboko, M.A.H. and Nakamura, E., 1996. Nd and Sr isotopic mapping of the Archaean-Proterozoic boundary in southeastern Tanzania using granites as probes for crustal growth. Precambrian Research, 77: 105-115.

Meinhold, K.D., 1970. Petrographie, Metamorphose, Tektonik und stratigraphische Stellung der Konse-Serie in Zentral-Tanzania (Ostafrica). Beihefte zom Geologischen Jahrbuch, 91: 1-137.

Möller, A., Appel, P., Mezger, K. and Schenk, V., 1995. Evidence for a 2 Ga subduction zone: eclogites in the Usagarian belt of Tanzania. Geology, 23: 1067-1070.

Möller, A., Mezger, K. and Schenk, V., 1998. Crustal age domains and the evolution of the continental crust in the Mozambique belt of Tanzania: combined Sm-Nd, Rb-Sr, and Pb-Pb isotopic evidence. Journal of Petrology, 39: 749-783.

Möller, A., Mezger, K. and Schenk, V., 2000. U-Pb dating of metamorphic minerals: Pan-African metamorphism and prolonged slow cooling of high pressure granulites in Tanzania, East Africa. Precambrian Research, 104: 123-146.

Molnar, P., 1992. Brace-Goetze strength profiles, the partitioning of strike-slip and thrust faulting at zones of oblique convergence, and the stree-heat paradox of the San Andreas Fault. In: B. Evans and T.-F. Wong (Editors), Fault Mechanics and Transport. Academic Press, New York, pp. 435-459.

Mount, V.S. and Suppe, J., 1992. Present-day stress orientations adjacent to active strike-slip faults: California and Sumatra. Journal of Geophysical Research-Solid Earth, 97: 11995-12013.

Mruma, A.H., 1989. Stratigraphy, Metamorphism and Tectonic evolution of the Early Proterozoic Usagaran belt, Tanzania. Res Terrae, A, no.2. University of Oulu, Finland.

Muhongo, S., Kröner, A. and Nemchin, A.A., 2001. Single zircon evaporation and SHRIMP ages for granulite-facies rocks in the Mozambique belt of Tanzania. Journal of Geology, 109: 171-189.

Nelson, D.R., 1997. Compilation of SHRIMP U-Pb zircon geochronology data, 1996. 1997/2, Geological Survey of Western Australia, Perth, Australia.

O'Nions, R.K., Hamilton, P.J. and Hooker, P.J., 1983. A Nd isotopic investigation of sediments related to crustal developments in the British Isles. Earth & Planetary Science Letters, 63: 229-240.

Peacock, S.M., 1993. The importance of blueschist-eclogite dehydration reactions in subducting oceanic crust. Geological Society of America, Bulletin, 105: 684-694.

Platt, J.P., 1993a. Exhumation of high-pressure rocks - a review of concepts and processes. Terra Nova, 5: 119-133.

Platt, J.P., 1993b. Mehanics of oblique convergence. Journal of Geophysical Research, 98: 16239-16256.

Priem, H.N.A. et al., 1979. Isotopic age determinations on granitic and gneissic rocks from the Ubendian-Usagaran System. Precambrian Research, 9: 227-239.

Reddy, S.M., Wheeler, J. and Cliff, R.A., 1999. The geometry and timing of orogenic extension: an example from the Western Italian Alps. Journal of Metamorphic Geology, 17: 573-589.

Richard, P. and Cobbold, P.R., 1990. Experimental insights into partitioning of fault motions in continental convergence wrench zones. Annales Tectonicae, IV: 35-44.

Ring, U., Brandon, M.T., Willett, S.D. and Lister, G.S., 1999. Exhumation Processes. In: U. Ring, M.T. Brandon, G.S. Lister and S.D. Willett (Editors), Exhumation Processes: Normal faulting, ductile flow and erosion. Geological Society Special Publication No. 154, pp. 1-28.

Ring, U., Kröner, A. and Toulkeridis, T., 1997. Palaeoproterozoic granulite-facies metamorphism and granitoid intrusions in the Ubendian-Usagaran orogen of northern Malawi, east-central Africa. Precambrian Research, 85: 27-51.

Roddick, J.C., Cliff, R.A. and Rex, D.C., 1980. The evolution of excess argon in Alpine biotites - a ^{40}Ar-^{39}Ar analysis. Earth & Planetary Science Letters, 48: 185-208.

Rubatto, D. and Gebauer, D., 2000. Use of cathodoluminescence for U-Pb zircon dating by ion microprobe: some examples from the western Alps. In: M. Pagel, V. Barbin, P. Blanc and D. Ohnenstetter (Editors), Cathodoluminescence in Geosciences. Springer-Verlag, Berlin.

Steiger, R.H. and Jager, E., 1977. Subcommission on geochronology: convention on the use of decay constants in geo- and cosmo-chronology. Earth and Planetary Science Letters, 36: 359-362.

Stern, R.A., 2002. Crustal evolution in the East African Orogen: a neodymian isotopic perspective. Journal Of African Earth Sciences, 34: 109-117.

Stern, R.J., 1994. Arc Assembly and continental collision in the Neoproterozoic East African orogeny - implications for the consolidation of Gondwana. Annual Review of Earth and Planetary Sciences, 22: 319-351.

Stevens Kalceff, M.A., Phillips, M.R., Moon, A.R. and Kalceff, W., 2000. Cathodoluminescence microcharacterisation of silicon dioxide polymorphs. In: M. Pagel, V. Barbin, P. Blanc and D. Ohnenstetter (Editors), Cathodoluminescence in Geosciences. Springer-Verlag, Berlin.

Suarez, G., Molnar, P. and Burchfiel, B.C., 1983. Seismicity, fault plane solutions, depth of faulting, and active tectonics of the Andes of Peru, Ecador and southern Colombia. Journal of Geophysical Research-Solid Earth, 88: 10404-10428.

Tikoff, B. and Greene, D., 1997. Stretching lineations in transpressional shear zones: an example from the Sierra Nevada Batholith, California. Journal of Structural Geology, 19: 29-39.

Tuisku, P. and Huhma, H., 1998. Eclogite from the SW-marginal zone of the Lapland Granulite belt: evidence from the 1.90-1.88 Ga subduction zone. In: E. Hanski and J. Vuollo (Editors), International Ophiolite Symposium and Field Excursion: Generation and Emplacement of Ophiolites Through Time. Geological Survey of Finalnd, Oulu, Finland, pp. 61.

Vernon, R.H. and Williams, P.F., 1988. Distinction between intrusive and extrusive or sedimentary parentage of felsic gneisses: Examples from the Broken Hill Block, NSW. Australian Journal Of Earth Sciences, 35: 379-388.

Wendt, I. et al., 1972. Age determinations of granitic intrusions and metamorphic events in the early Precambrian of Tanzania. 24th International Geological Congress, Montreal - section 1: 295-314.

Whittingham, J.K., 1954. Geological map of Nyanzwa-south B37/S 1. Quarter degree sheet 198. Geological Survery Department, Dodoma.

Whittingham, J.K., 1959. The Geology of the Nyanzwa Area. Bulletin of the Geological Survey of Tanganyika, 27 pp.

Figures Captions

Figure 1. Map showing the location of the Usagaran Orogen in Tanzania. The box indicates the location of the study area. L. Tan = Lake Tanganyika.

Figure 2. Geological Map of part of the Usagaran Orogen, Tanzania. Map and lithological subdivisions are after Mruma (1989) and Whittingham (1954). The box indicates the location of the study area and corresponds to the boundaries of Figs. 4 and 5. Yalumba Hill, along strike of the rocks studied here, contains well preserved eclogite-facies assemblages (Möller et al., 1995).

Figure 3. Photographs of structural features seen in the Isimani Suite, Great Ruaha River. Long side of card scale is 9cm. Domains 1 to 5 refer to structural domains identified in Fig. 4. a) S_1 compositional banding and composite S_1/S_2 foliation folded by NW-verging F_3 fold in domain 1. b) S_2 foliation surface (XY plane) with well-developed mineral elongation and mineral aggregate lineation (L_2). c) S_2 foliation with σ-porphyroclasts of quartz and feldspar in an amphibolite layer of domain 1. Photograph taken looking at XZ section. Sense of shear is top-to-NW (left) d) S_2 foliation in XZ section of domain 3. δ-porphyroclast of quartz indicates sinistral shear sense (top-to-left in photo). Lens cap has a diameter of 55mm. e) Zone of localised high strain D_2 deformation overprinting lower strain but still strongly foliated and folded migmatitic gneiss in domain 3. The lower strain zone is interpreted to preserve the earlier stages of the D_2 deformation (see text for details). f) Isoclinal F_2 fold

refolded by NW verging F_3 folds in compositionally banded (S_1) leucocratic gneiss. A younger D_4 extensional shear clearly cuts the F_3 axial surfaces. g) D_4 extensional structure cutting compositionally banded leucocratic gneiss. Main D_4 structure has normal top-to-SE displacement. Inset shows detail of antithetic extensional structures which developed synchronously with the main structure. h) Large scale extensional shear zone (D_4) showing top-to-SE shear located at the boundary of domains 4 and 5. Circle indicates location of hammer for scale.

Figure 4. Structural map of the Isimani Suite exposed in the Great Ruaha River section. Stereonets are lower hemisphere equal area projections and show the geometry of S_2 and L_2 in five identified structural domains recognised both on geometry and kinematic evidence (see text for detail). Inset stereonets indicate the orientations of F_2 and F_3 structural elements. Location of younger D_4 and D_5 structures are shown in grey. Grid refers to UTM sheet 37M.

Figure 5. Map and cross section illustrating the kinematics of Isimani deformation. Most data relates to the kinematics of the D_2 deformation. The zone of "ambiguous kinematic data" arises due to poorly developed and inconsistent kinematic indicators in this area. Location of D_4 and D_5 structures are also shown.

Figure 6. Map-view illustration of a complex D_2 structure in domain 3 of the Isimani Suite. Close F_2 folds that deform S_1 are cut by a syn-D_2 mafic igneous unit that is subsequently deformed by further high strain D_2 deformation at its margins. The intrusion of the competent mafic unit leads to the localised preservation of the early stages of the D_2 deformation path in its strain shadow (see text for details).

Figure 7. Characteristic cathodoluminescence (CL) images of T01-01 (a, b and c) and T01-24b (d). All ages quoted are ^{204}Pb corrected, ^{207}Pb/^{206}Pb ages. a) Type 1 zircon grain (grain "a" in Table 1) from Kidete Hill intrusion. Euhedral form with narrow oscillatory CL zones demonstrating a broad light to dark, core to rim transition. b) A subhedral Type 2 zircon (analysis 21 in Table 1): a xenocryst core rimmed with a thin mantle of brightly luminescing zircon. c) A complex xenocryst (Type 3, grain "b" in Table 1) with a core of Archaean zircon mantled with <80 Ma younger zircon in a complex series of overlapping rims. d) Three zircons from T01-24b, Isimani granitic gneiss. Numbers refer to analyses spots detailed in Table 1. Numbers refer to analyses in Table 1. The apparently younger cores in both these dated grains correlate with high U+Th contents and probably reflect partial resetting during annealing of metamict zircon.

Figure 8. a) U-Pb concordia plot of zircons from sample T01-01. Two discordia are drawn, one very precise line is based primarily on Type 1 zircons, the upper intercept is interpreted to date the crystallisation age of the granite. The older discordia is less well constrained, but is identical (within error) to the age of the Isimani granite gneiss (T01-24b; Fig. 8b). b) U-Pb concordia plot of zircons from sample T01-24b. The filled ellipses were not used to construct the discordia curve, and are interpreted either as xenocrysts incorporated in the original magma or as discordant grains that lost Pb during the Neoproterozoic East African Orogeny. Inset shows a cumulative probability plot of $^{207}Pb/^{206}Pb$ ages that are <10% discordant, both histograms and Gaussian relative probability curves are shown, the y-axis scale refers to the histogram. The plot illustrates that there is a significant spread in age of the grains that define the upper discordia/concordia intercept suggesting one extended period, or multiple periods of zircon formation.

Figure 9. Summary diagram illustrating the combined effects of three end-member models to explain the geometry and kinematic variations of the high strain D_2 Isimani deformation (refer text for details). "K" schematically illustrates the relationship of deformation to intrusion of the 1871 Ma Kidete Granite. "X" indicates the direction of mineral elongations, interpreted to represent the orientation of maximum stretch of the finite strain ellipse within each domain. Interpreted kinematic vorticity axes are also shown. Interspersed domains of well-developed and ambiguous kinematics may reflect the localisation of simple and pure shear components respectively (Model 1). Domains recording different kinematics may have developed at different times during a single progressive deformation in which strain becomes localised as deformation progresses (Model 2). The different domains may also have developed during reactivation of early formed structures either at amphibolite and/ or greenschist facies conditions (Model 3).

Table Captions

Table 1: U-Pb SHRIMP data. '%com. ^{206}Pb' is the percentage of non-radiogenic ^{206}Pb in the measured total. Ages are in Ma, with errors quoted at 1σ. 'C' represents core analyses, 'R' represents rim analyses. Numbers (1-3) associated with T01/01 refer to zircon type – see text for details. Letters in the column labelled "Grain" indicate grains where more than one analysis was undertaken on the same zircon grain. **x** = not used in calculating the discordia line.

Samples run on the SHRIMP II based at the John de Laeter Centre for Excellence in Mass Spectrometry in Perth, Australia
Common Pb derived from measured ^{204}Pb and assuming a Broken Hill Pb isotopic ratio

Spot	Grain	Spot type	Conc. (ppm) U	Th	$^{232}Th/^{238}U$	%com. ^{206}Pb	$^{206}Pb^2/^{238}U$	$\pm^3$	$^{208}Pb^2/^{232}Th$	$\pm^3$	$^{207}Pb^2/^{206}Pb$	$\pm^3$	Ages $^{206}Pb^2/^{238}U$	$\pm^3$	$^{208}Pb^2/^{232}Th$	$\pm^3$	$^{207}Pb^2/^{206}Pb$	$\pm^3$	% disconc.
Data processed using the programs SQUID and ISOPLOT by Ken Ludwig																			
Kidete granite: T01-01																			
T01.01		2	610	82	0.14	0.04	0.4440	3.2200	11.1975	3.2337	0.1829	0.2974	2369	64	2512	85	2679	5	13
T01.02		3,C	965	70	0.07	0.02	0.5137	3.1844	13.0072	3.1920	0.1836	0.2206	2672	70	2423	97	2686	4	1
T01.03	a	1, R	600	335	0.58	1.32	0.2473	3.2174	3.8127	3.7150	0.1118	1.8574	1424	41	2288	84	1829	34	28
T01-04		2	342	156	0.47	0.18	0.5190	1.6863	13.4211	1.7603	0.1876	0.5049	2695	37	2561	51	2721	8	1
T01-05		1, C	2244	1440	0.66	0.10	0.4106	1.7442	10.3698	1.7588	0.1832	0.2263	2218	33	2474	64	2682	4	21
T01-06		1	2567	1058	0.43	0.08	0.3404	1.5638	5.4107	1.5965	0.1153	0.3211	1889	26	1943	32	1884	6	0
T01-07		3	431	121	0.29	3.81	0.0373	1.8472	0.5347	7.5339	0.1041	7.3040	236	4	789	44	1699	135	620
T01-08	a	1, C	328	306	0.96	1.40	0.2750	1.7043	4.3304	2.7143	0.1142	2.1126	1566	24	2067	51	1867	38	19
T01-09		1, R	479	257	0.55	0.84	0.3143	1.9481	4.8572	2.6676	0.1121	1.8223	1762	30	2132	65	1834	33	4
T01-10		1	80	46	0.60	4.98	0.1625	2.3570	1.8926	12.7660	0.0845	12.5466	971	21	1504	123	1303	244	34
T01-11		1, C	665	378	0.59	0.15	0.5559	1.6258	15.2772	1.6974	0.1993	0.4876	2850	37	2817	52	2820	8	-1
T01-12		1	350	498	1.47	0.20	0.3190	1.9158	5.0162	2.0585	0.1140	0.7531	1785	30	1756	43	1865	14	4
T01-13	b	3, R	493	189	0.40	0.18	0.4853	1.6266	12.4879	1.6844	0.1866	0.4374	2550	34	1970	38	2713	7	6
T01-14	b	3, C	1482	146	0.10	0.08	0.5313	1.5721	14.3178	1.6098	0.1955	0.3461	2747	35	2522	80	2789	6	2
T01-15		2	3265	721	0.23	0.06	0.5122	1.5559	13.1922	1.6101	0.1868	0.4143	2666	34	2775	51	2714	7	2
T01-16		2	805	1264	1.62	0.35	0.4854	1.5997	12.2592	1.7291	0.1832	0.6565	2551	34	1148	32	2682	11	5
T01-17		1	171	96	0.58	0.70	0.3064	1.7697	4.8426	2.3041	0.1146	1.4755	1723	27	1743	45	1874	27	9
T01-18		1	194	161	0.86	4.41	0.4557	1.9860	6.6865	5.9308	0.1064	5.5884	2421	40	3914	132	1739	102	-28
T01-19		1	2934	2249	0.79	0.11	0.3475	1.5701	5.4883	1.6176	0.1146	0.3891	1922	26	1968	34	1873	7	-3
T01-20		1	4783	4604	0.99	0.07	0.3646	1.5522	5.7671	1.5748	0.1147	0.2661	2004	27	1988	32	1875	5	-6
T01-21		2	1327	265	0.21	0.41	0.4401	1.7080	11.1093	1.8170	0.1831	0.6198	2351	34	457	104	2681	10	14
T01-22		1	1964	1338	0.70	0.04	0.3295	1.7807	5.2219	1.8053	0.1149	0.2968	1836	28	1839	35	1879	5	2
T01-23	c	1, C	3613	1608	0.46	0.55	0.2596	1.5612	4.0894	1.6931	0.1142	0.6553	1488	21	1642	29	1868	12	26
T01-24	c	1, R	342	129	0.39	0.85	0.2262	1.7004	3.4055	2.4288	0.1092	1.7342	1314	20	1678	53	1786	32	36
T01-25	b	3, R	725	185	0.26	0.14	0.4818	1.5982	12.3122	1.6639	0.1853	0.4631	2535	33	2298	69	2701	8	7
T01.26		2	535	72	0.14	0.04	0.4511	1.6569	11.3736	1.6836	0.1829	0.2989	2400	33	2547	50	2679	5	12
T01.27		2	846	61	0.07	0.03	0.5254	1.5935	13.3021	1.6089	0.1836	0.2222	2722	35	2471	73	2686	4	-1
T01.28		1	526	293	0.58	1.36	0.2526	1.6443	3.8554	2.5701	0.1107	1.9752	1452	21	2335	57	1811	36	25

Spot	Grain	Spot type	Conc. (ppm) U	Th	$^{232}Th/^{238}U$	%com. ^{206}Pb	$^{206}Pb^2/^{238}U$	±[3]	$^{208}Pb^2/^{232}Th$	±[3]	$^{207}Pb^2/^{206}Pb$	±[3]	Ages $^{206}Pb^2/^{238}U$	±[3]	$^{208}Pb^2/^{232}Th$	±[3]	$^{207}Pb^2/^{206}Pb$	±[3]	% disconc.
Isimani Orthogneiss: T01-24b																			
T24b-01	**x**		347	281	0.84	0.02	0.5746	3.1871	16.5717	3.2118	0.2092	0.3975	2927	75	2821	91	2899	6	-1
T24b-02	a, **x**	C	3936	1423	0.37	1.69	0.0957	3.3020	2.2194	3.5827	0.1682	1.3903	589	19	679	47	2540	23	331
T24-03	a	R	719	167	0.24	0.01	0.5117	3.1664	13.1433	3.1746	0.1863	0.2280	2664	69	2645	85	2710	4	2
T24-04			214	128	0.62	0.23	0.4891	3.2038	12.5331	3.2391	0.1859	0.4769	2567	68	1544	56	2706	8	5
T24-05	b	C	534	95	0.18	0.03	0.4997	3.1736	12.8765	3.2020	0.1869	0.4256	2613	68	2563	89	2715	7	4
T24-06	b	R	378	84	0.23	0.07	0.5139	3.2283	13.2681	3.2465	0.1872	0.3435	2673	71	2505	89	2718	6	2
T24-07	**x**		224	112	0.52	0.11	0.3498	3.4090	7.5294	3.4765	0.1561	0.6819	1933	57	1764	100	2414	12	25
T24b-08	c	C	1014	346	0.35	0.32	0.3198	3.3039	7.9662	3.3415	0.1807	0.4998	1789	52	2123	77	2659	8	49
T24b-09	c	R	801	244	0.31	0.02	0.4928	3.2079	12.7674	3.2172	0.1879	0.2454	2583	68	2338	77	2724	4	5
T24b-10	d, **x**	C	3037	69	0.02	2.27	0.1861	3.1867	4.1835	3.8415	0.1630	2.1452	1100	32	6508	1183	2487	36	126
T24b-11	d	R	1745	300	0.18	0.68	0.2905	3.6350	7.0992	3.7010	0.1773	0.6958	1644	53	1970	130	2627	12	60
T24b-12			493	163	0.34	0.03	0.4711	3.4720	11.8839	3.4854	0.1830	0.3051	2488	72	2298	82	2680	5	8
T24b-13	e, **x**	C	1022	776	0.78	0.36	0.5251	3.2780	15.2261	3.2922	0.2103	0.3050	2721	73	2576	92	2908	5	7
T24b-14	e	R	1351	356	0.27	0.16	0.3873	3.1641	9.8110	3.1726	0.1837	0.2321	2110	57	1950	64	2687	4	27
T24b-15			3994	1255	0.32	2.52	0.0982	3.1648	1.9001	3.8720	0.1403	2.2308	604	18	1106	48	2231	39	270
T24b-16	f	C	230	89	0.40	0.10	0.4466	3.2183	10.9589	3.5623	0.1780	1.5273	2380	64	2256	77	2634	25	11
T24b-17	f, **x**	R	840	201	0.25	3.11	0.3367	3.1785	7.7680	3.9520	0.1673	2.3486	1871	52	2368	194	2531	39	35
T24b-18	**x**		464	223	0.50	0.05	0.4517	3.2251	12.2476	3.2638	0.1966	0.5011	2403	65	2326	78	2799	8	16
T24b-19			378	95	0.26	0.19	0.4292	3.1842	10.7275	3.2121	0.1813	0.4225	2302	62	1606	60	2665	7	16
T24b-20			3254	380	0.12	0.62	0.1505	3.1998	3.4793	3.2852	0.1676	0.7442	904	27	998	93	2534	12	180
T24b-21	g, **x**	C	761	74	0.10	0.08	0.4938	3.1699	13.3425	3.1801	0.1960	0.2543	2587	68	2414	128	2793	4	8
T24b-22	g	R	844	266	0.33	0.02	0.5076	3.2164	13.0352	3.2270	0.1862	0.2617	2646	70	2651	86	2709	4	2
T24b-23			357	170	0.49	0.07	0.5066	3.2273	12.7894	3.2636	0.1831	0.4855	2642	70	2598	86	2681	8	1
T24b-24			4238	2019	0.49	0.50	0.1615	3.6244	3.8322	3.6537	0.1721	0.4618	965	32	1066	40	2579	8	167
T24b-25			1163	82	0.07	0.04	0.4844	3.2019	12.3480	3.2082	0.1849	0.1997	2546	67	2090	110	2697	3	6
T24b-26			900	165	0.19	0.32	0.2391	3.3395	5.6553	3.3677	0.1716	0.4350	1382	42	1412	58	2573	7	86
T24b-27	h, **x**	C	616	72	0.12	0.04	0.3765	3.2681	8.9045	3.2835	0.1715	0.3166	2060	58	2041	98	2573	5	25
T24b-28	h	R	1699	157	0.10	0.01	0.5097	3.1977	12.8970	3.2022	0.1835	0.1695	2655	70	2760	133	2685	3	1
T24b-29			261	152	0.60	0.26	0.3406	3.2036	8.1208	3.2580	0.1729	0.5929	1890	52	1028	38	2586	10	37
T24b-30	**x**		692	172	0.26	0.09	0.3522	3.1721	8.0237	3.1964	0.1652	0.3929	1945	53	1872	61	2510	7	29

Reddy et al. Tectonophysics
Figure 1

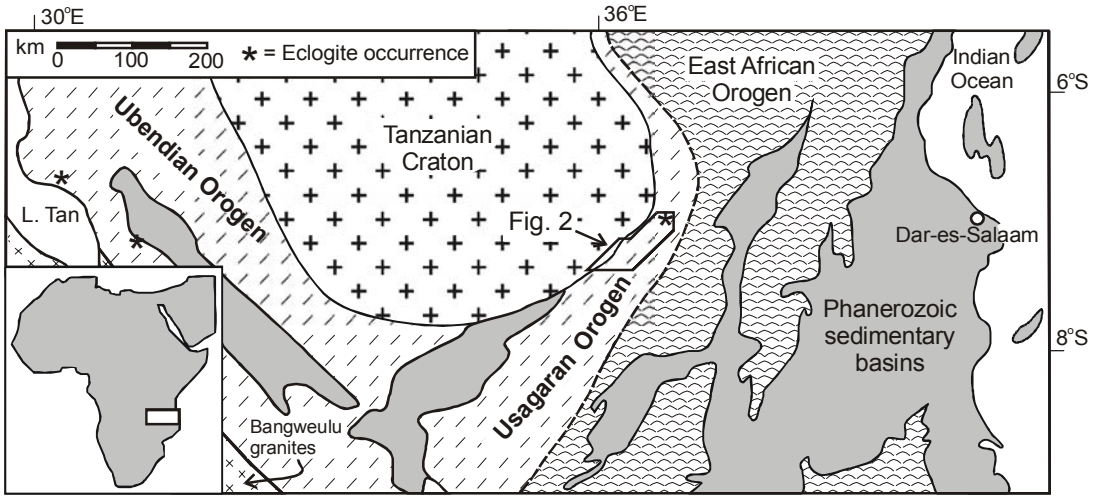

Reddy et al. JAES
Figure 2

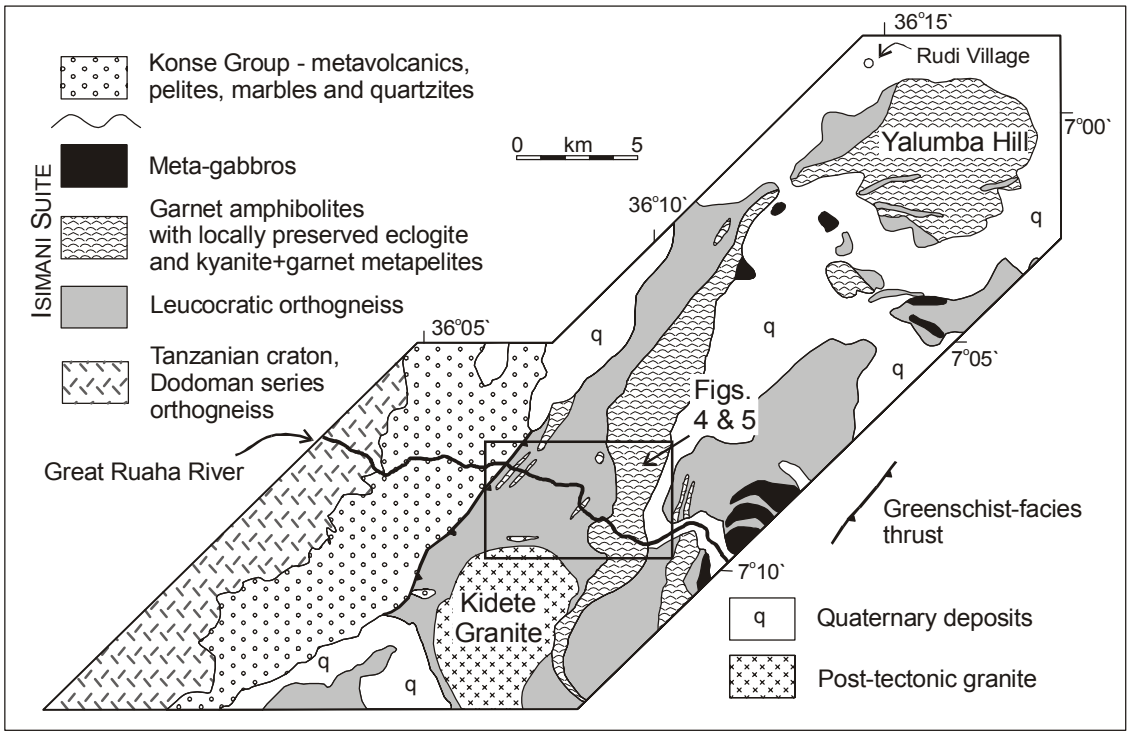

Reddy et al. / Tectonophysics
Figure 3

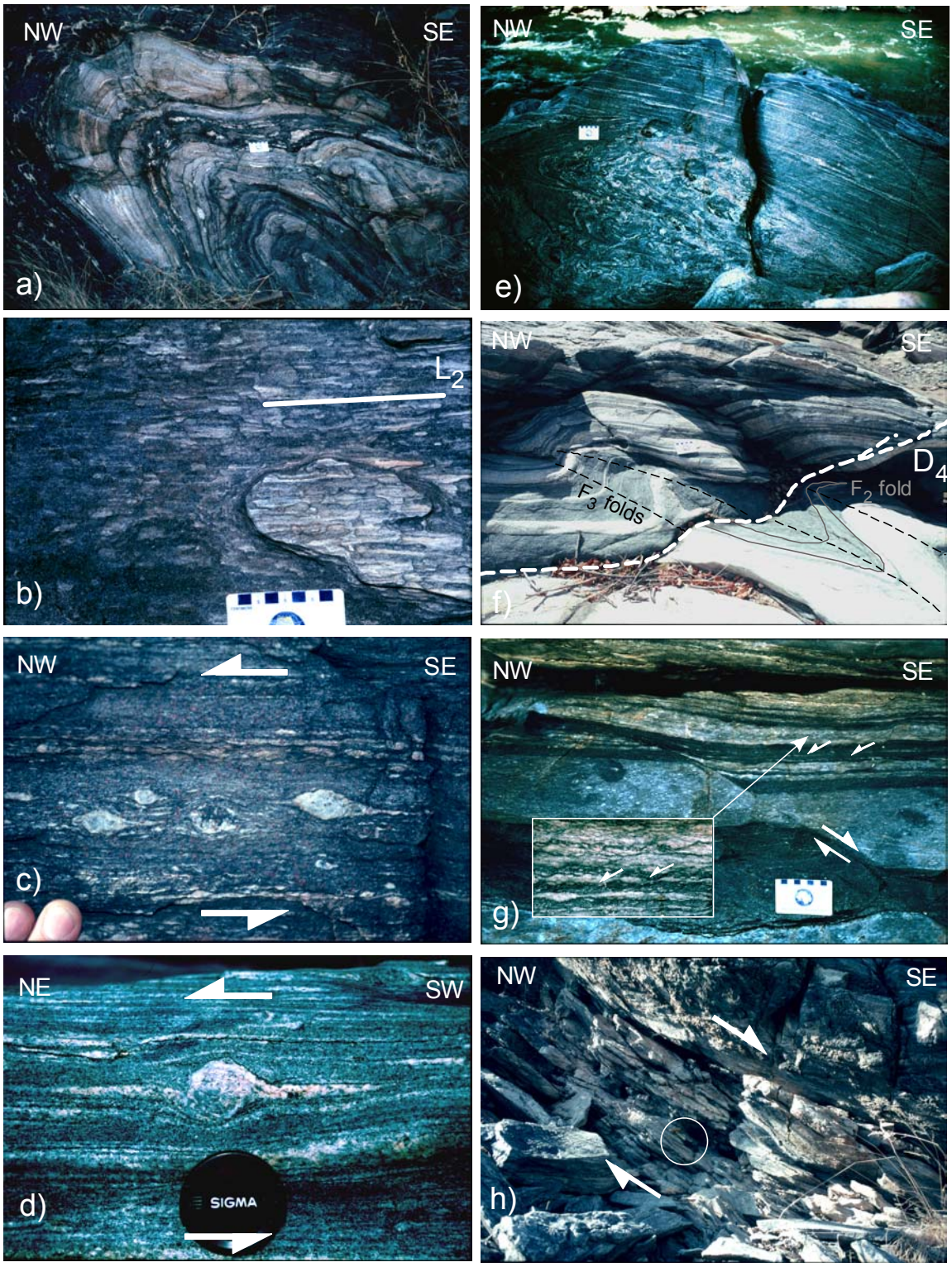

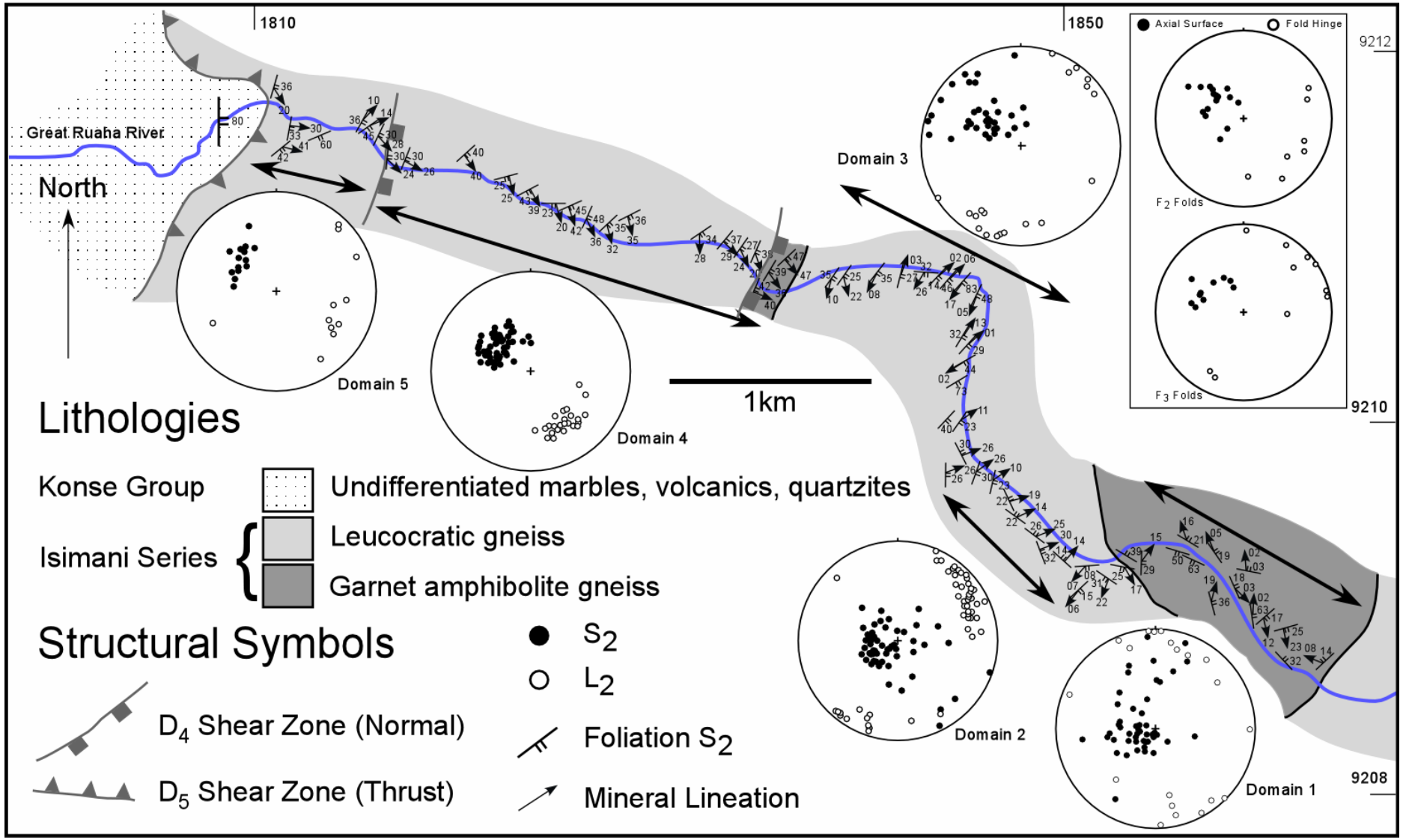
1810
1850
9212
9210
9208
Great Ruaha River
North
Domain 1
Domain 2
Domain 3
Domain 4
Domain 5
1km
Axial Surface
Fold Hinge
F2 Folds
F3 Folds
Lithologies
Konse Group
Undifferentiated marbles, volcanics, quartzites
Isimani Series
Leucocratic gneiss
Garnet amphibolite gneiss
Structural Symbols
S2
L2
D4 Shear Zone (Normal)
D5 Shear Zone (Thrust)
Foliation S2
Mineral Lineation

Reddy et al / Tectonophysics
Figure 5

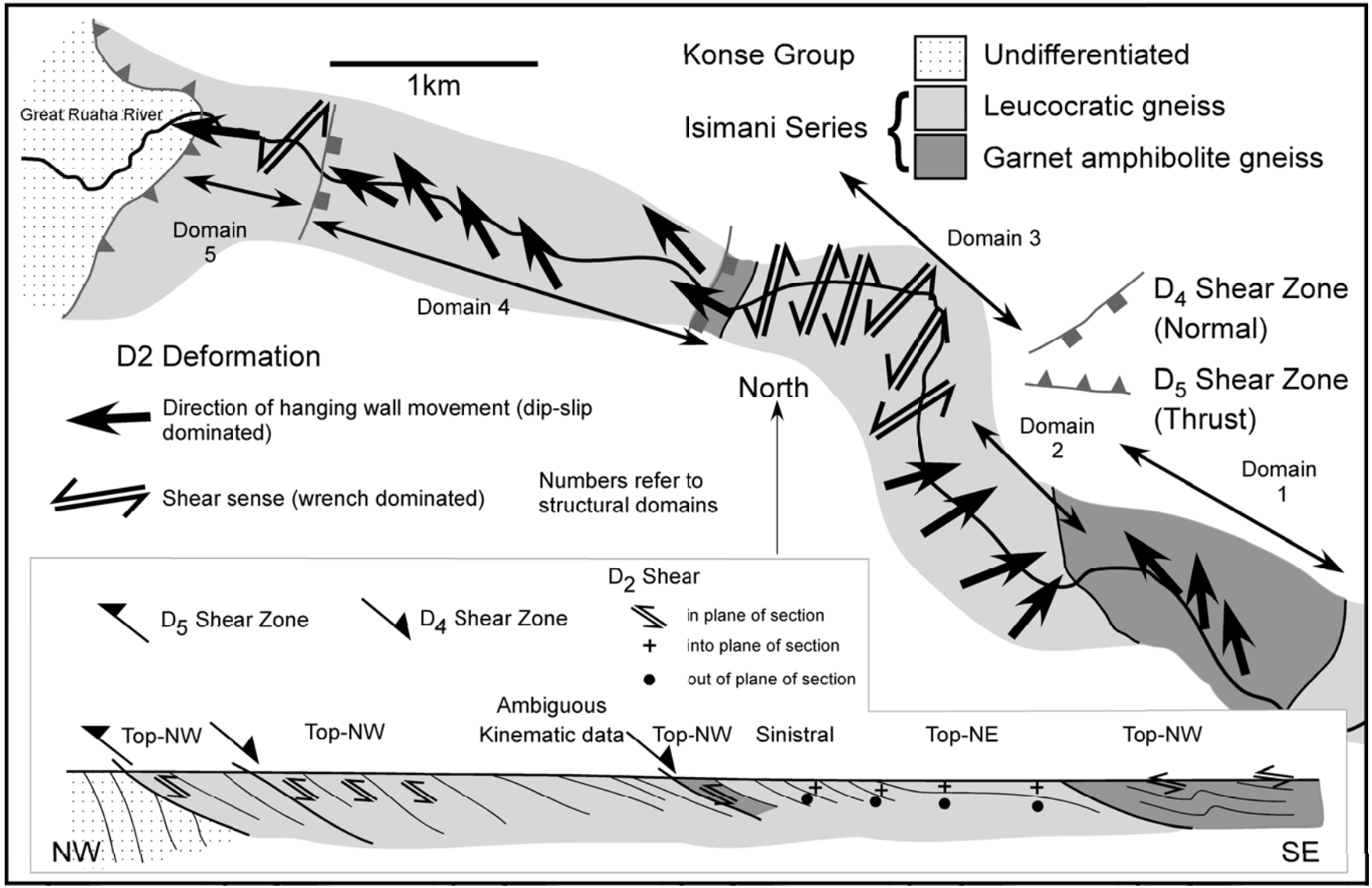

Reddy et al. / Tectonophysics
Figure 6

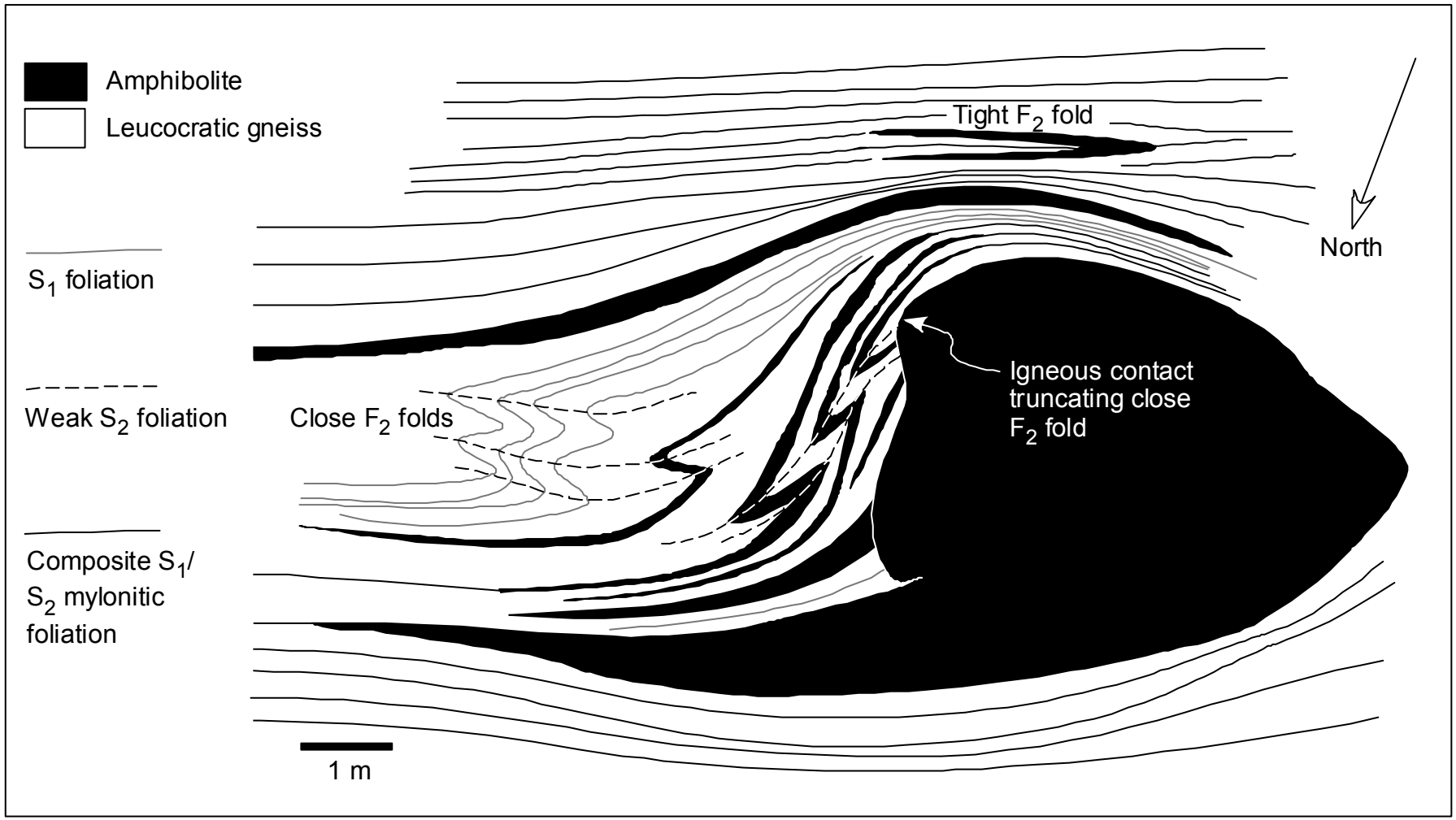

Reddy et al. Tectonophysics
Figure 7

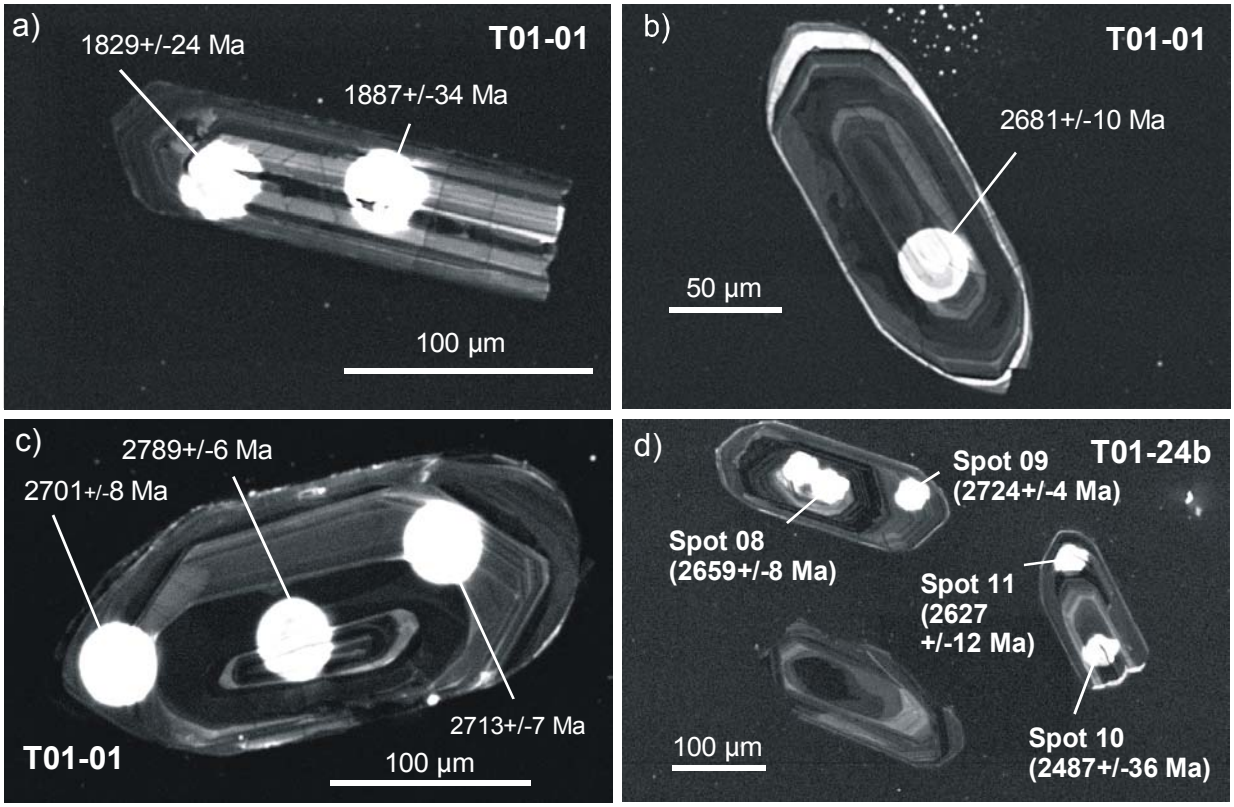

Reddy et al., Tectonophysics
Figure 8

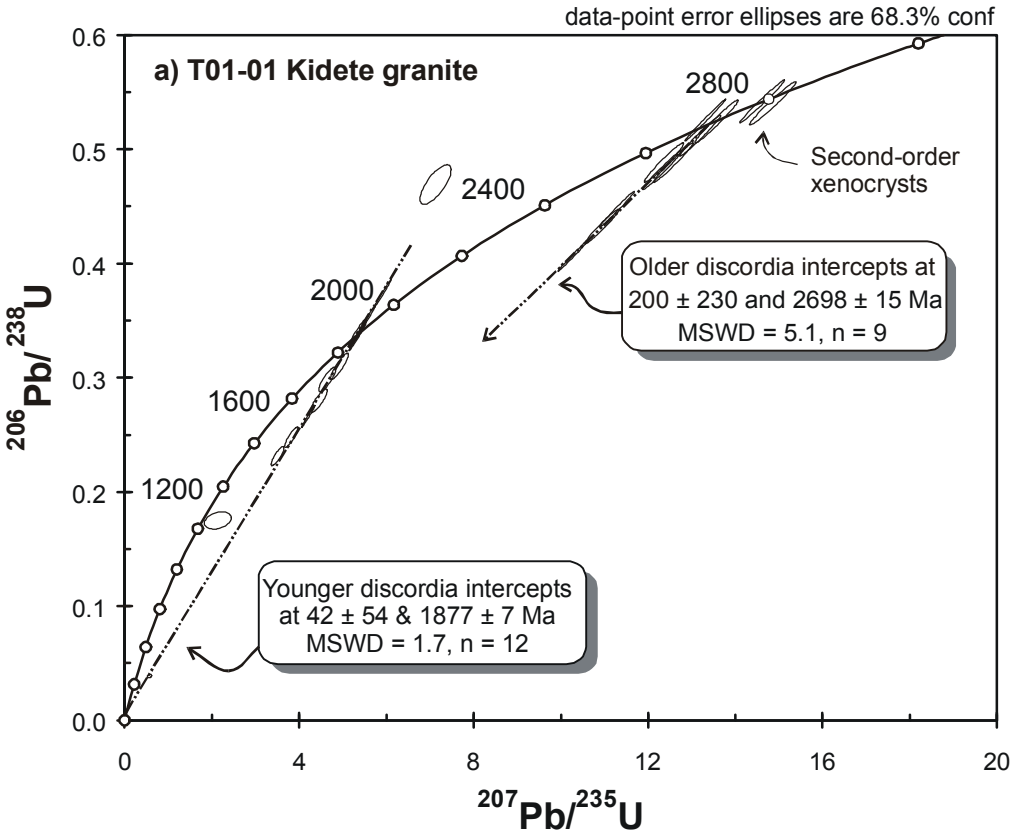

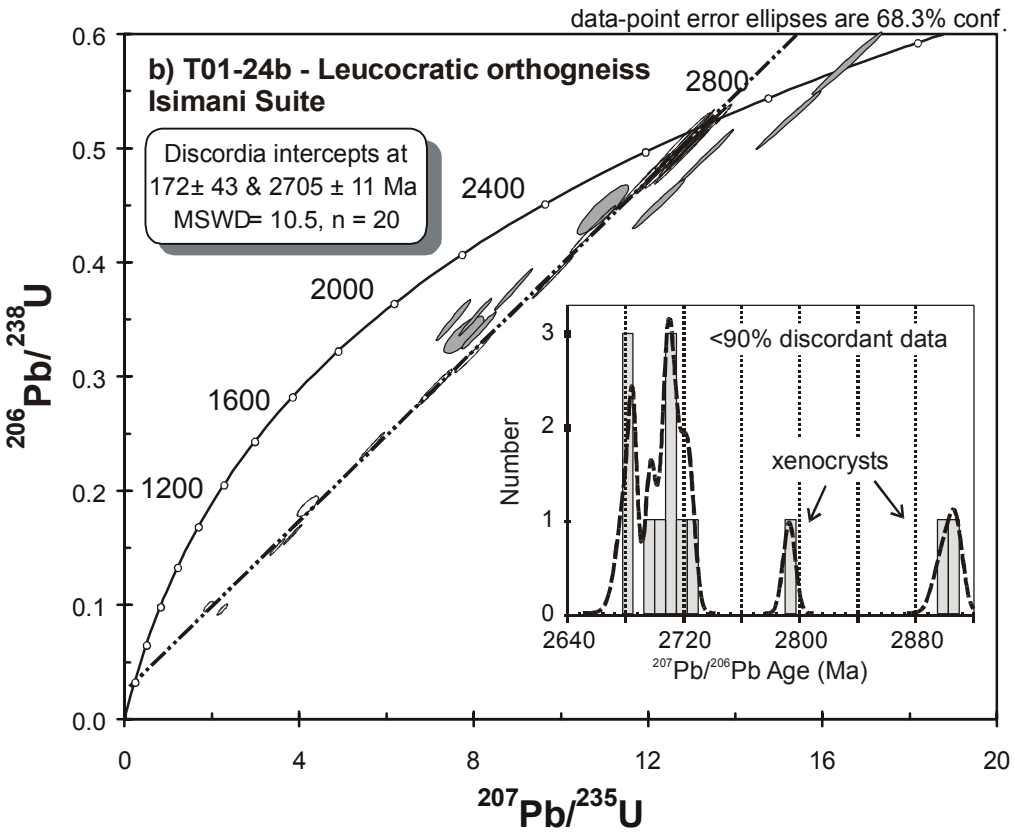

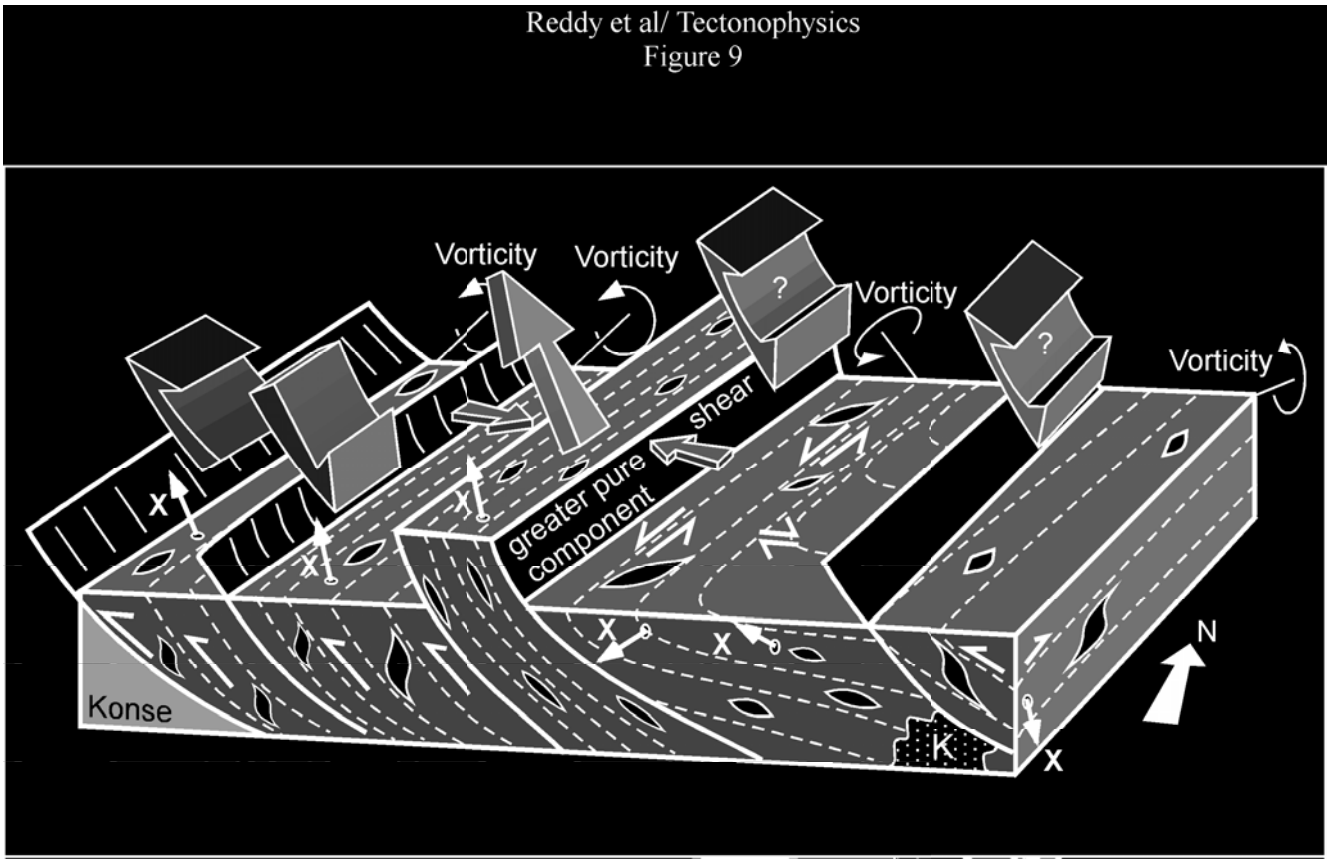
Reddy et al/ Tectonophysics
Figure 9
Vorticity
Vorticity
Vorticity
Vorticity
?
?
shear
greater pure
component
Konse
K
N
X
X
X
X